# scientific reports

OPEN

# mTORC2 interactome and localization determine aggressiveness of high-grade glioma cells through association with gelsolin

Naphat Chantaravisoot [1,2,11]✉, Piriya Wongkongkathep[2,3,11], Nuttiya Kalpongnukul[2], Narawit Pacharakullanon[1], Pornchai Kaewsapsak[1,4], Chaiyaboot Ariyachet[1,5], Joseph A. Loo[6,7,8], Fuyuhiko Tamanoi[9,10] & Trairak Pisitkun[2,3]✉

mTOR complex 2 (mTORC2) has been implicated as a key regulator of glioblastoma cell migration. However, the roles of mTORC2 in the migrational control process have not been entirely elucidated. Here, we elaborate that active mTORC2 is crucial for GBM cell motility. Inhibition of mTORC2 impaired cell movement and negatively affected microfilament and microtubule functions. We also aimed to characterize important players involved in the regulation of cell migration and other mTORC2-mediated cellular processes in GBM cells. Therefore, we quantitatively characterized the alteration of the mTORC2 interactome under selective conditions using affinity purification-mass spectrometry in glioblastoma. We demonstrated that changes in cell migration ability specifically altered mTORC2-associated proteins. GSN was identified as one of the most dynamic proteins. The mTORC2-GSN linkage was mostly highlighted in high-grade glioma cells, connecting functional mTORC2 to multiple proteins responsible for directional cell movement in GBM. Loss of GSN disconnected mTORC2 from numerous cytoskeletal proteins and affected the membrane localization of mTORC2. In addition, we reported 86 stable mTORC2-interacting proteins involved in diverse molecular functions, predominantly cytoskeletal remodeling, in GBM. Our findings might help expand future opportunities for predicting the highly migratory phenotype of brain cancers in clinical investigations.

According to the 2016 World Health Organization (WHO) classification system, glioblastoma multiforme (GBM) has been classified as a grade IV type of diffuse astrocytic tumor and divided into subgroups depending on their molecular profiles[1]. GBM is the most malignant type of glioma and one of the most deleterious human cancers based on its low overall survival (OS) of approximately 15 months, estimated 10-year survival rate of 0.71%, high recurrence rates after diagnosis, and resistance to both chemotherapy and radiotherapy. Despite multiple aggressive treatments, most cases experience recurring tumors and finally progress to death[2–4].

The mechanistic target of rapamycin complex 2 (mTORC2) has been implicated as one of the major signaling molecules in various types of brain cells and an attractive therapeutic target for GBM[5–7]. mTORC2 mainly consists

[1]Department of Biochemistry, Faculty of Medicine, Chulalongkorn University, 1873 Rama IV Pathumwan, Bangkok 10330, Thailand. [2]Center of Excellence in Systems Biology, Faculty of Medicine, Chulalongkorn University, Bangkok 10330, Thailand. [3]Research Affairs, Faculty of Medicine, Chulalongkorn University, Bangkok 10330, Thailand. [4]Research Unit of Systems Microbiology, Faculty of Medicine, Chulalongkorn University, Bangkok 10330, Thailand. [5]Center of Excellence in Hepatitis and Liver Cancer, Faculty of Medicine, Chulalongkorn University, Bangkok 10330, Thailand. [6]Department of Chemistry and Biochemistry, University of California, Los Angeles, CA 90095, USA. [7]UCLA/DOE Institute of Genomics and Proteomics, University of California, Los Angeles, CA 90095, USA. [8]Department of Biological Chemistry, University of California, Los Angeles, CA 90095, USA. [9]Department of Microbiology, Immunology and Molecular Genetics, University of California, Los Angeles, CA 90095, USA. [10]Institute for Integrated Cell-Material Sciences, Institute for Advanced Study, Kyoto University, Kyoto 606-8501, Japan. [11]These authors contributed equally: Naphat Chantaravisoot and Piriya Wongkongkathep. ✉email: naphat.c@chula.ac.th; trairak@gmail.com

of mTOR kinase, RICTOR, MAPKAP1 (or mSIN1), and MLST8[8]. Growth factors can stimulate mTORC2, resulting in AKT phosphorylation at serine 473[9]. This multiprotein complex has been identified as a crucial regulator of actin cytoskeleton reorganization through PKCα phosphorylation and other PKC isoforms[10–12].

The relationship between the deregulated mTORC2 signaling pathway and the malignancy of gliomas has been increasingly reported as more mTORC2 functions are revealed[13–15]. Hyperactivation of mTORC2 has also been observed in clinical samples from multiple cancers in various studies[16–21]. Moreover, the inhibition of mTORC2 by several ATP-competitive mTOR kinase inhibitors and RICTOR/mTORC2 depletion could decrease the cell growth, proliferation, motility, invasiveness, and stemness properties of GBM cells and malignant glioma tumors[22–25]. Dysregulated mTORC2 signaling has been associated with metabolic reprogramming events in GBM[26,27]. mTORC2 phosphorylates FLNA at its stabilizing residue (S2152), promoting the migration and invasion of GBM cells through the interactions of FLNA and integrins at the plasma membrane[22,28]. Nevertheless, the mechanisms by which mTORC2 may interact with other proteins to directly control cancer cell motility have not been thoroughly investigated.

Proteomic studies of GBM have been extensively performed in several aspects, mainly to determine biomarkers[29–31]. Quantitative proteomics has become a powerful method for identifying valid predictive biomarkers for brain cancers[32]. Moreover, mass spectrometry has emerged to characterize protein–protein interactions (PPIs) in disease or drug perturbations[33]. However, none of the proteomic studies in GBM focuses explicitly on its highly migratory characteristics or mTORC2-mediated directional migration of cancer cells.

Here, we aim to extensively decipher the mTORC2 interactome and the mechanisms underlying how mTORC2 promotes highly migratory characteristics of GBM cells. Using quantitative proteomics and systems biology approaches, we demonstrate that mTORC2 interacts with all types of the cytoskeleton and that its cellular localization indicates cancer cells' ability to promote migration. Comparative analyses of the proteomic data sets of high- and low-grade glioma cells were combined to screen for vital regulators responsible for glioblastoma's enhanced motility. Finally, we identified GSN as one of the distinct players connecting mTORC2 to several actin-binding and microtubule-associated proteins. Our work comprehensively provides proven evidence of direct and indirect PPIs between mTORC2 and cytoskeleton-associated proteins that could generate the complex network initiating the regulation of cytoskeletal dynamics.

## Results

### mTORC2 is a crucial regulator of glioblastoma migration.
To confirm the regulation of the mTORC2 signaling cascade in GBM cells, we performed western blotting analysis of the U87MG whole-cell lysate to show that growth factors can substantially activate mTORC2 signaling in cells by inducing pAKT (S473), while amino acids did not elevate pAKT level. In contrast, both serum and amino acids could stimulate mTORC1 signaling by increasing the level of pS6 (S235/236). Additionally, we showed that AZD8055, an ATP-competitive mTOR inhibitor, could inhibit both mTORC1 and mTORC2 by significantly reducing pS6 and pAKT levels, respectively. Nevertheless, rapamycin, a conventional mTOR inhibitor, potently inhibited only mTORC1 (Fig. 1A). Then, we investigated the dose-dependent effects of AZD8055 on the phosphorylation of mTORC2 downstream targets. We found that the amounts of pFLNA (S2152), pAKT (S473), and pS6 (S235/236) were significantly decreased at concentrations above 0.2 μM, and the most effective condition was 2.0 μM (Fig. 1B). Since AZD8055 is highly specific to mTOR kinase at concentrations up to 10 μM[34], we selected the treatment condition at 2.0 μM as the main concentration for all experiments. We showed that RICTOR siRNA treatment decreased the levels of the activated mTORC2 effectors pFLNA and pAKT (Fig. 1C). Next, to emphasize the significance of mTORC2 signaling in GBM cell migration control, we observed the migration ability of U87MG cells under different culturing conditions. U87MG cells under serum starvation, treated with AZD8055 or siRICTOR, showed impaired migration compared with cells in the activated state, while rapamycin did not decrease the migration rate (Fig. 1D,E). The results suggested that mTORC2 plays a primary role in supporting GBM cell motility.

Moreover, we performed live-cell imaging to investigate cell migration behavior when mTORC2 was blocked. The wound-healing assay results showed that cells treated with AZD8055 could not close the gap efficiently, and their directional migration was disrupted, as shown by the tangled cell tracking lines (Fig. 1F, Supplementary Video 1). Subsequently, 24-h RICTOR-knockdown and serum-starved cells were tested to investigate whether activating mTORC2 complexes by growth factors could restore cell migration ability. We replaced the serum-deprived culture media with DMEM containing 10% FBS and found that the cancer cells closed the gap within 18 h after media replacement. Conversely, serum-starved cells did not acquire migration capability (Fig. 1G, Supplementary Video 2). Our findings have concluded that active mTORC2 is critical for the migration of GBM cells.

### Inactivation of mTORC2 affects actin cytoskeleton and microtubule network architecture and dynamics.
To better understand the causes of GBM cell impaired migration after mTORC2 activity was disrupted, we first investigated actin cytoskeleton dynamics when cells were treated with AZD8055 by live-cell imaging (Fig. 1H, Supplementary Video 3). The results showed that when mTORC2 complexes were inhibited, the actin network was highly affected, leading to abnormal migration. We observed significantly fewer actin filaments surrounding the AZD8055-treated cell membrane region. Therefore, we hypothesized that the loss of organized actin networks near the plasma membrane (PM) prevented cells from moving regularly. In addition, we proposed that microtubule dynamics might also be defective when migrational control is strongly inhibited under mTORC2-suppressing conditions. We aimed to explore the effects on the overall structures of the actin cytoskeleton and microtubules using live-cell fluorescence imaging. U87MG cells treated with AZD8055 and siRICTOR, except for rapamycin, showed a considerably nonfunctional, abnormal cytoskeleton. Apart from damaged actin filaments, the shrinkage of microtubules was also observed. The fluorescently labeled β-tubulin proteins appeared mainly in the perinuclear area, suggesting that cells could not extend their microtubules to the
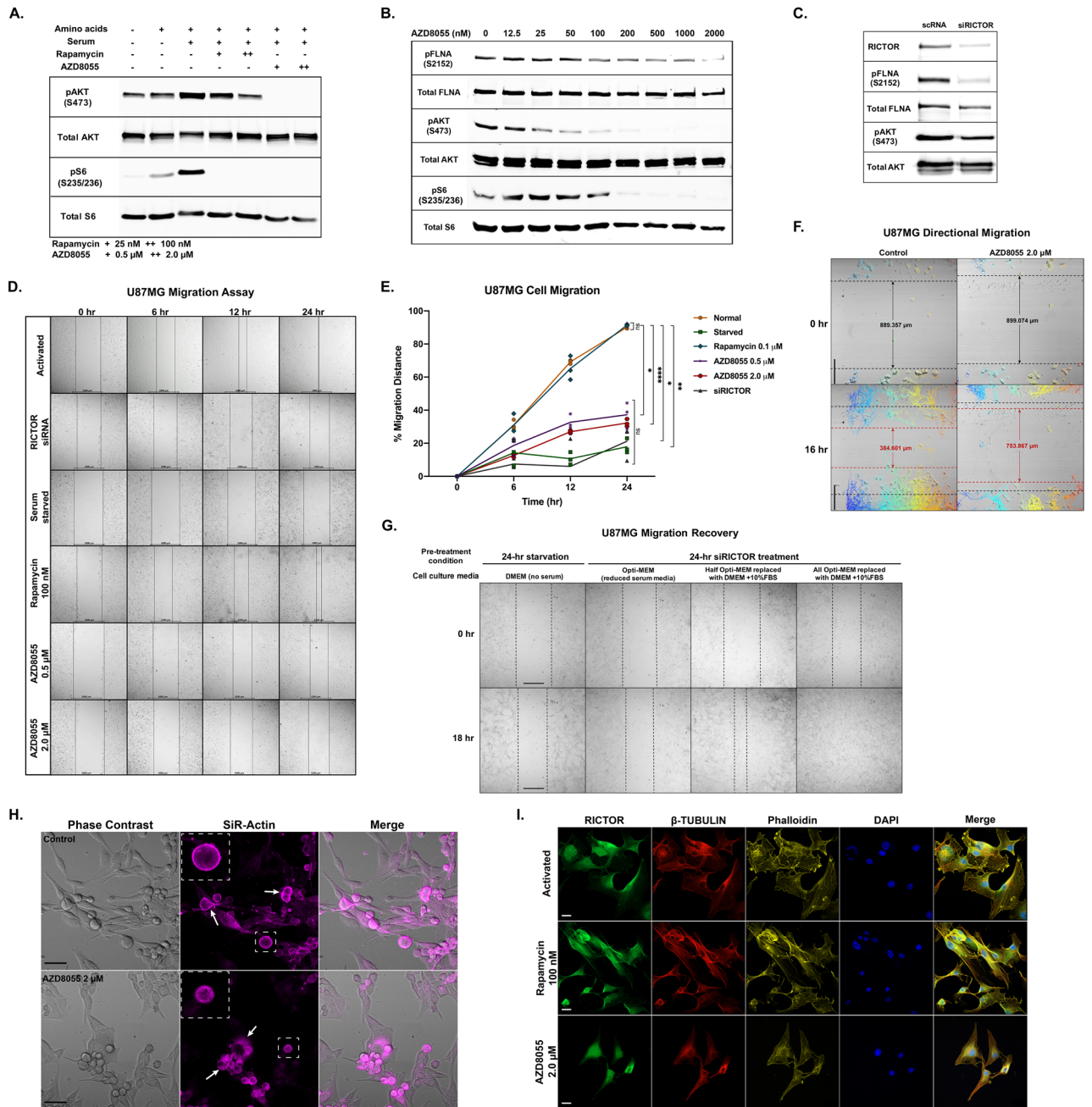
**Figure 1.** mTORC2 signaling pathway and cell migrational control in U87MG cells. **(A)** Western blot showing activation of mTORC1 (pS6) and mTORC2 (pAKT) by amino acids and serum and inhibition by rapamycin and AZD8055. **(B)** Western blot showing dose-dependent inhibition of mTORC1 (pS6) and mTORC2 (pFLNA and pAKT) by AZD8055. **(C)** Western blot analysis of RICTOR, pFLNA, and pAKT showing mTORC2 kinase activities after *RICTOR* knockdown. **(D)** Wound-healing migration assays of U87MG cells under activation and inhibition (siRICTOR, serum starvation, 100 nM rapamycin, 0.5 μM and 2.0 μM AZD8055) conditions at 0, 6, 12, and 24 h. Scale bar, 100 μm. **(E)** Migration distance percentage quantification of U87MG cells under different culturing conditions shown in (D); n = 3. Statistical significance was calculated at the endpoint (24 h) using two-way ANOVA with Tukey's multiple-comparisons test comparing each treated group with the normal group: * $p < 0.05$, ** $p < 0.01$, *** $p < 0.001$, **** $p < 0.0001$, ns = not significant. **(F)** Directional migration (16 h) of normal and 2.0 μM AZD8055-treated U87MG cells. Colored-tracking lines represent the migrating direction of each cell in a circle. Scale bar, 200 μm. See also Video S1. **(G)** Cell migration recovery by serum supplementation (18 h) of siRICTOR-treated cells. Scale bar, 100 μm. See also Video S2. **(H)** Snapshot from live-cell imaging of U87MG cells containing actin labeled with SiR-Actin under normal and AZD8055-treated conditions. See also Video S3. Scale bar, 20 μm. **(I)** Immunofluorescence staining of F-actin and the microtubules of activated, rapamycin-treated (100 nM, 24 h), and AZD8055-treated (2.0 μM, 24 h) U87MG cells. Scale bar, 20 μm.

PM. (Supplementary Fig. 1; Supplementary Video 4, 5). We suspected that active mTORC2 might interact with tubulin isoforms and microtubule-associated proteins to control microtubule dynamics.

We further confirmed this observation by staining F-actin and β-tubulin with RICTOR proteins. We discovered that RICTOR localization was altered from a concentrated amount near the PM in the activated cells to nuclear and perinuclear regions in AZD8055-treated cells. In contrast, GBM cells treated with rapamycin did not exhibit any distinct changes (Fig. 1I). Overall, the results indicated that active mTORC2 might promote cell migration by physically interacting with microtubules, microfilaments, and cytoskeletal accessory proteins.

### mTORC2 complex integrity is critical for its localization.

Since RICTOR colocalizes with FLNA in GBM cells and mTORC2 inhibition causes FLNA dissociation from the actin cytoskeleton[22], we hypothesized that the localization of RICTOR and FLNA would be changeable depending on mTORC2's activation status. We found that RICTOR and FLNA localized differently in starved and AZD8055-treated cells compared to activated cells (Fig. 2A). We later explored whether RICTOR could represent the whole mTORC2 complex. Immunofluorescence (IF) staining of the main components of mTORC2, mTOR, RICTOR, and MAPKAP1, showed that all proteins colocalized near the cell membrane under the mTORC2-activating state. In contrast, starvation and AZD8055 treatment resulted in fewer PM-linked mTORC2 complexes. Additionally, the three proteins only
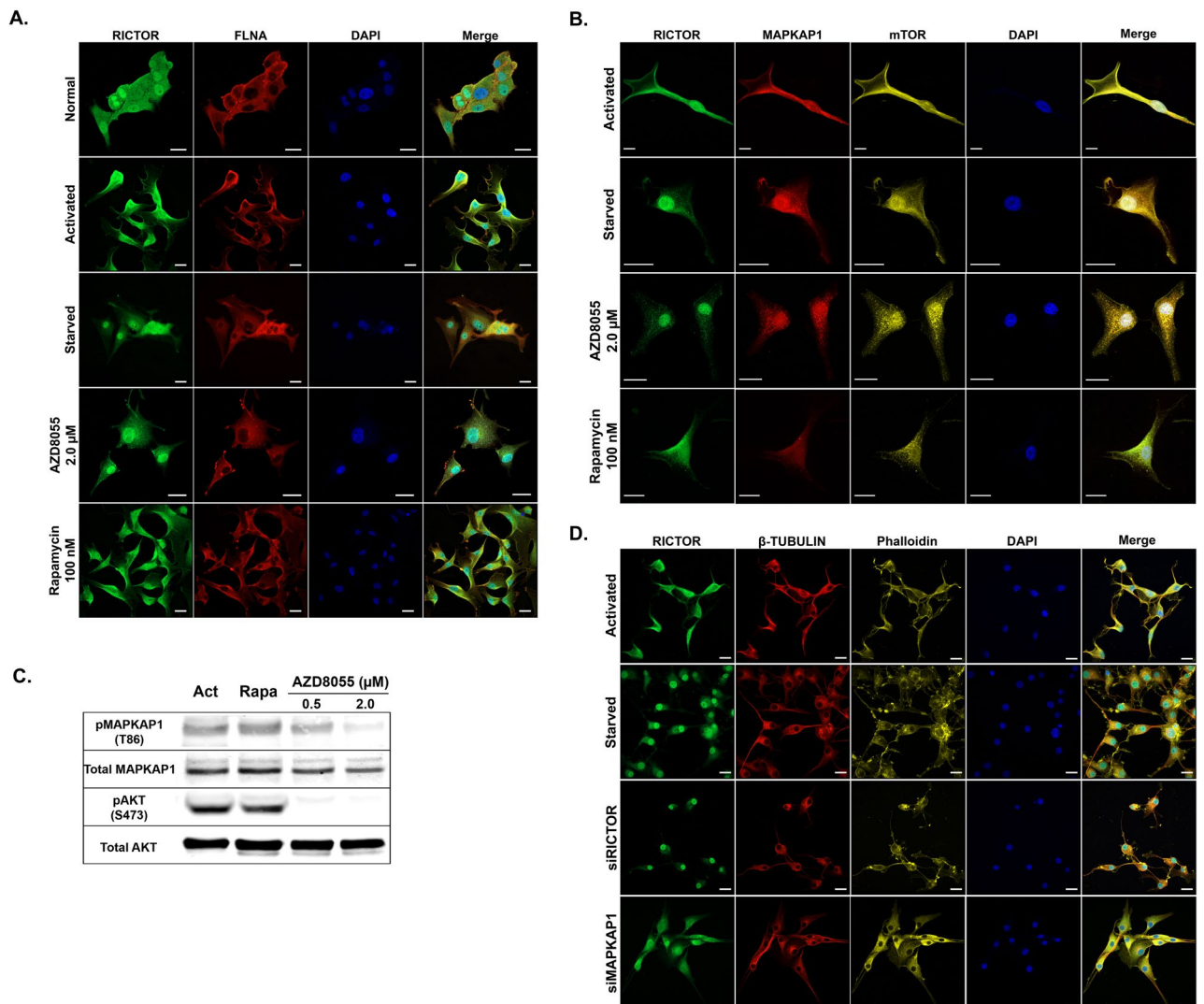


**Figure 2.** mTORC2 localization, integrity, and effects on cytoskeleton rearrangement. **(A)** Immunofluorescence analysis showing localization of RICTOR and FLNA proteins in U87MG cells under normal, activating, and three inhibition conditions. Scale bar, 20 μm. **(B)** Immunofluorescence analysis showing the localization of RICTOR, MAPKAP1, and mTOR proteins in U87MG cells under activating and three inhibitory conditions. Scale bar, 20 μm. **(C)** Western blot analysis showing mTORC2 complex integrity (pMAPKAP1) and activity (pAKT) in U87MG cells treated with rapamycin and AZD8055 compared to activation conditions. **(D)** Immunofluorescence analysis showing the localization of RICTOR and the characteristics of F-actin (phalloidin) and microtubules (β-TUBULIN) in U87MG cells under activation and knockdown conditions (siRICTOR and siMAPKAP1 treatments). Scale bar, 20 μm.

partially colocalized in both inactivation conditions (Fig. 2B). However, rapamycin did not affect RICTOR-MAPKAP1 colocalization. Our results correlated with a previous study showing that rapamycin does not affect mTORC2 assembly[35]. Hence, the results suggested that the functionally active mTORC2, associated with a highly migratory phenotype, is localized at the PM.

In addition, the distribution of mTORC2 can contribute to the regulation of its kinase activity. For example, the membrane recruitment of mTORC2 sufficiently promotes AKT phosphorylation[10,36,37]. Additionally, MAPKAP1 was shown to initiate the binding of mTORC2 to the cell membrane[38]. Thus, we examined the amount of pMAPKAP1 at T86, referring to mTORC2 complex integrity, in U87MG cells under different treatments[39,40]. We detected a similar amount of pMAPKAP1 (T86) in the activated and rapamycin-treated cells but a significantly lower amount in AZD8055-treated cells. Therefore, under migration-promoting conditions, mTORC2 was intact, functionally active, and existed near the cell membrane (Fig. 2C). Regarding our hypothesis, we performed IF staining of RICTOR, F-actin, and β-tubulin in U87MG cells. Under an activation condition, an elevated signal of RICTOR was detected near the PM. In contrast, the cells from the three inactivation conditions exhibited an impaired cytoskeleton, while RICTOR proteins were absent from the PM area (Fig. 2D). These experiments emphasized the importance of active mTORC2 in driving the directional motility of GBM cells, leading to the next question of which mechanisms mTORC2 could directly induce a well-organized cytoskeleton promoting U87MG migration.

### mTORC2 interactome supports the complex's function in brain cancer cell motility.

To gain further mechanistic insights into mTORC2-mediated cell migration promotion, we aimed to comprehensively characterize the interacting partners of mTORC2 by affinity purification-mass spectrometry (AP-MS) method. We used an anti-RICTOR antibody coupled with protein A magnetic beads to pull down endogenous mTORC2 and its associated proteins (Fig. 3A). To identify specific RICTOR interactors, we performed quantitative immunoprecipitation combined with knockdown (QUICK)[33] to compare siRICTOR-treated and normal cells.

We expected to identify all mTORC2-associated proteins in samples from the normal condition but decreased or absent in the *RICTOR* knockdown (KD) group (Fig. 3B). RICTOR and mTOR were reduced in the siRICTOR-treated immunoprecipitated (IP) product, while the mTOR amount in the whole-cell lysate was not affected (Fig. 3C). We performed label-free quantitative proteomic analysis and reported 309 proteins proximally associated with RICTOR (Supplementary Table 1). A volcano plot was created from 122 proteins commonly found in both conditions (Fig. 3D,E). The RICTOR amount was depleted by more than seven-fold. We successfully pulled down the known key components of mTORC2, including RICTOR, mTOR, MAPKAP1, and MLST8, as well as FLNA and MYH9, which we reported previously[22]. We also found 17 other known interacting proteins of RICTOR based on the GPS-PROT database[41], as shown in Supplementary Table 1. We characterized the mTORC2 interactome using DAVID Bioinformatics Resources 6.8 tools. The top-ranked enriched Gene Ontology terms (GOCC, GOBP, and GOMF) passing the 5% false discovery rate (FDR) cut-off were selected and are shown in Fig. 3F. Focusing on cell migration regulation, we found that the identified proteins consisted of actin, actin-binding proteins, tubulin isoforms, microtubule-associated proteins, intermediate filaments, and other cytoskeletal regulatory proteins (Fig. 3G). Thus, we could infer that mTORC2 physically interacted with three types of the cytoskeleton and might directly regulate the dynamics of the cytoskeletal networks affecting the migratory phenotypes of GBM cells.

### Quantitative proteomics reveals specific interacting partners of RICTOR in U87MG cells with various migratory abilities.

Since we observed that mTORC2 altered its intracellular localization when inactivated, we hypothesized that distinct groups of proteins would be highly associated with mTORC2 depending on its activation status. Therefore, we determined all proteins interacting with mTORC2 in two groups of cells with two distinguishable phenotypes, motile and nonmotile, using mass spectrometry. AP-MS experiments were performed using U87MG cells cultured under three different conditions: serum starvation (ST), serum activation (ACT), and AZD8055 treatment (AZD). We compared $\log_2$-transformed label-free quantification (LFQ) intensity of identified proteins from the two pairs: (1) ACT and ST and (2) AZD and ACT. More proteins were identified in the ACT eluate than in the ST and AZD eluates (Fig. 4A, Supplementary Tables 2–4). We supposed that the upregulated and uniquely found proteins in the ACT group would provide more information about how mTORC2 controls cell motility. The LFQ intensity comparisons between the common proteins found in all repeats of each pair of conditions are represented as volcano plots (Fig. 4B,C, Supplementary Tables 5, 6). Significantly increased proteins of ACT/ST with $\log_2$ fold change over two include myosin-9 (MYH9), myosin-1D (MYO1D), gelsolin (GSN), plectin (PLEC), and ATP-binding cassette subfamily F member 2 (ABCF2). Moreover, MYH9, MYO1D, microtubule-associated protein 1B (MAP1B), and actin, cytoplasmic 2 (ACTG1) were significantly decreased in the AZD/ACT group. Note that GSN and ABCF2 were absent from the RICTOR IP of AZD8055-treated cells (Supplementary Table 7). We also found that when starved or inhibited by AZD8055, MAPKAP1 was missing from the mTORC2 IP product (Supplementary Table 7), as previously shown that inactive mTORC2 did not contain MAPKAP1[42–44]. However, in GBM cells, we observed that mTOR and RICTOR were substantially intact under inhibitory conditions.

Associated enriched GO terms were annotated to the mTORC2 interactome increased or present after mTORC2 activation (ACT/ST) and decreased or absent after the inhibition of mTORC2 (AZD/ACT) (Fig. 4D,E). We observed that a group of identical proteins (shown as orange circles in volcano plots) was inversely regulated, suggesting that these proteins interacted with active mTORC2 and consequently dissociated after mTORC2 inactivation or vice versa (Supplementary Table 8). Proteins that were statistically less associated with active mTORC2 but tended to bind more to inactive mTORC2 complexes consisted of intermediate filament proteins
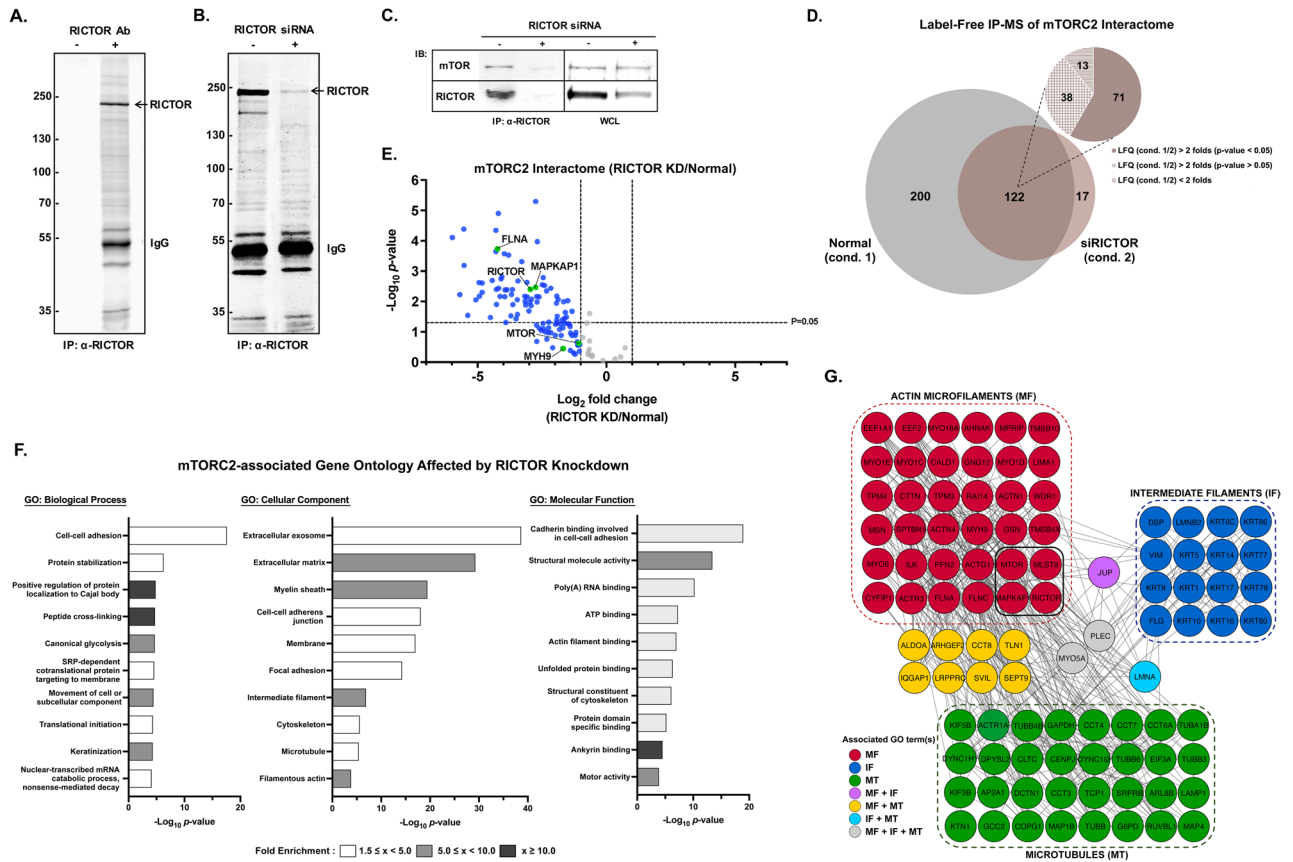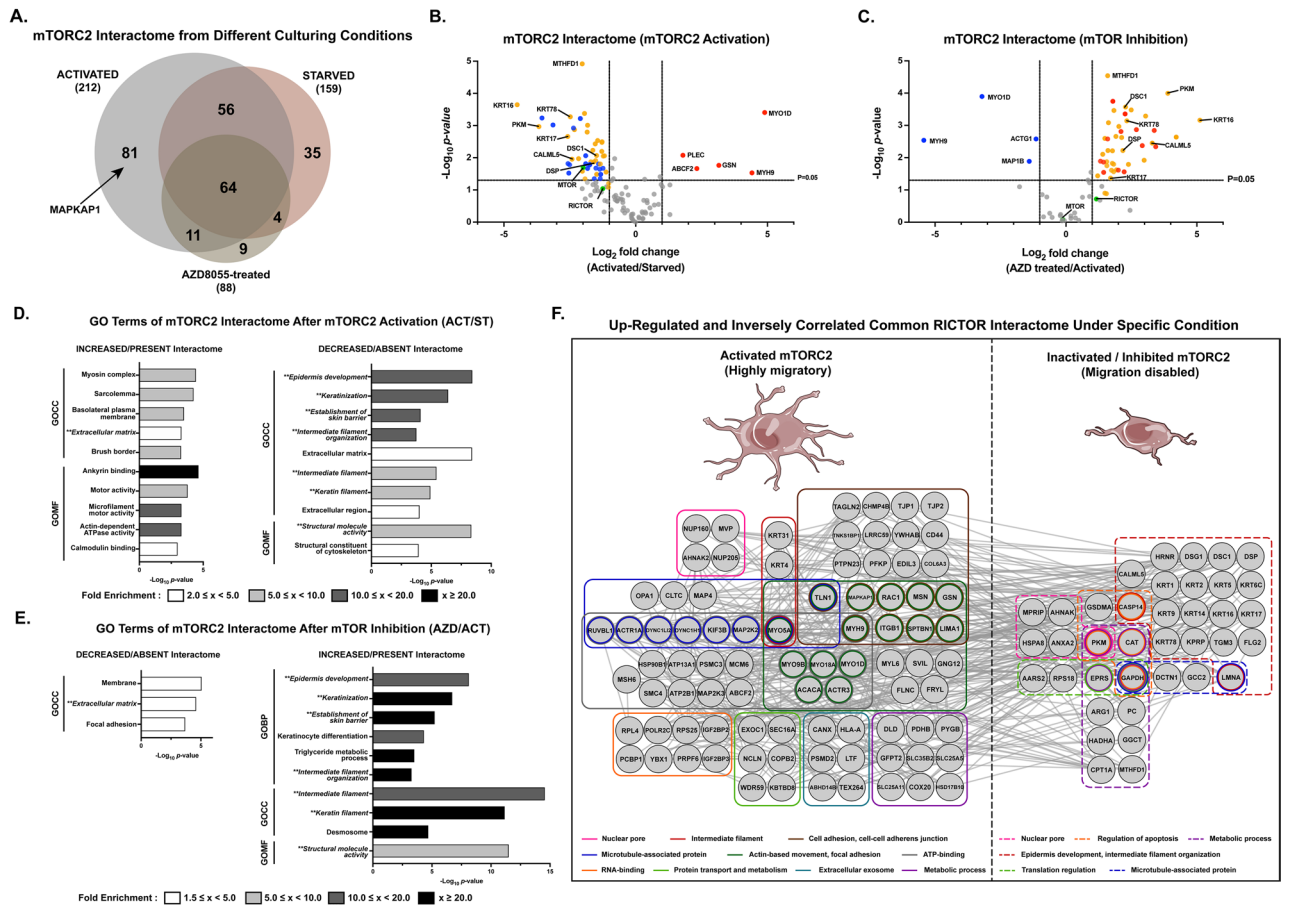
**Figure 3.** Identification of the mTORC2 interactome by AP-MS. **(A)** Coomassie-stained SDS-PAGE gel of an immunoprecipitation assay using protein A magnetic beads incubated with or without anti-RICTOR antibody. **(B)** Coomassie-stained SDS-PAGE gel of RICTOR-IP comparing the control U87MG cells and siRICTOR-treated cells. **(C)** Western blot analysis of immunoprecipitated RICTOR samples and whole-cell lysate (WCL) of U87MG cells treated with RICTOR siRNA compared to the control. **(D)** mTORC2-interacting proteins identified by AP-MS analysis compared between normal and *RICTOR* knockdown cells as in (B); n = 3 biological replicates. **(E)** Volcano plots of the results of the AP-MS experiment in (D) showing mTORC2-associated proteins affected by *RICTOR* knockdown. Proteins with a fold change (LFQ siRICTOR/normal) ≥ 2 are shown in blue. Known mTORC2 components and interacting proteins are shown in green circles. **(F)** Gene ontology analysis of 309 proteins negatively affected by *RICTOR* knockdown (decreased by at least twofold or absent in siRICTOR-treated IP samples). Ten top-ranked -log$_{10}$($p$-value) GOBP, GOCC, and GOMF terms with FDR < 0.05 are shown. **(G)** mTORC2-interacting protein–protein network based on cytoskeleton-associated proteins from blue circles in (E) affected by *RICTOR* knockdown. Proteins associated with each group of the cytoskeleton were labeled with different colors. Known key components of mTORC2 are in the black-bordered square.

such as the keratin isoforms and desmosome components. A network of upregulated mTORC2-interacting partners promoting each phenotypic characteristic determining cell movement was created (Fig. 4F).

### High-grade and low-grade glioma cells have different acquired migration capabilities and RICTOR intracellular localization.

Next, we compared the phenotypic changes acquired in GBM relative to their less invasive counterpart, low-grade glioma. We investigated and compared various characteristics of two cell lines: a nontumorigenic low-grade glioma cell line (H4) and a glioblastoma (grade IV glioma) cell line (U87MG).

Western blotting analysis showed that U87MG and H4 cell lines expressed comparable amounts of RICTOR. Both cell lines had high mTORC2 activities according to their pAKT (S473) levels, although slightly lower in H4. The effects of AZD8055 and rapamycin on mTORC2 activity were similar (Fig. 5A). Then, we performed a cell proliferation assay and observed that H4 cells were as highly proliferative as U87MG cells and were slightly more resistant to AZD8055 (Supplementary Fig. 2A). Hence, the cell proliferation rate of the cell lines could not distinguish brain cancer cells according to their aggressiveness.

Moreover, we compared the migration of H4 and U87MG cells (the U87MG migration assay is shown in Fig. 1F). H4 cells migrated approximately three times slower than U87MG cells (Fig. 5B, Supplementary Fig. 2B). We later determined the localization of RICTOR and FLNA inside the H4 cells and found that they were primarily localized around the perinuclear and nuclear regions, which is different from U87MG cells (Fig. 5C).

**Figure 4.** Quantification of the mTORC2 interactome under cell migration-associated conditions. (**A**) Overlap of the mTORC2 interactome identified from AP-MS experiments performed in U87MG cells under activated, starved, and 2.0 μM AZD8055-treated conditions. (**B,C**) Volcano plots of the results of AP-MS experiments in (**A**) showing changes in mTORC2-associated proteins by serum-stimulated mTORC2 activation in (**B**) and AZD8055-mediated mTOR inhibition in (**C**); n = 3 biological replicates. Proteins with $\log_2$ fold change (LFQ ACT/ST or LFQ AZD/ACT) ≥ 1, $p < 0.05$ are highlighted in red, while proteins with $\log_2$ fold change ≤ -1, $p < 0.05$ are highlighted in blue. Statistical significance was calculated from the LFQ values of each common protein of the two conditions using an unpaired two-sided Student's t-test. Green circles are known mTORC2-associated proteins. Inversely regulated identical proteins downregulated in ACT/ST and upregulated in AZD/ACT are shown in orange. (**D,E**) Gene ontology analysis of the mTORC2 interactome increased/present and decreased/absent by mTORC2 activation (**D**) and mTOR inhibition (AZD8055 treatment) (**E**). Top-ranked $-\log_{10}(p$-value) GOBP, GOCC, and GOMF terms with FDR < 0.05 are shown, and the bar colors represent the fold enrichment of each specific term. (**F**) Protein–protein interaction network of the mTORC2 interactome upregulated in each specific condition with the distinguished phenotype (activated/highly migratory or inhibited/migration disabled) and found to be downregulated in the opposite condition. All candidate proteins shown in the network were significantly changed with fold change ≥ 2 and $p$-value < 0.05. Proteins were categorized into various groups labeled by different colors depending on their common associated biological processes, cell components, or functions. Circles with two or more colors represent proteins related to several gene ontologies.

## AP-MS characterizes distinct mTORC2 interactome profiling of high-grade and low-grade glioma.

Since we expected to pinpoint specific interacting partners prevailing in the superior migration of U87MG cells, label-free quantitative proteomic analyses of H4 and U87MG whole-cell lysates were performed. A total of 2733 common proteins were retrieved. For cell line-specific proteins, we identified 523 proteins from H4 cells and 16 proteins from U87MG cells. The cytoskeleton-associated proteins exclusively found in each group are listed (Supplementary Fig. 2C). The common 1310 proteins identified from all replicates of both cells were compared and are shown in the volcano plot (Fig. 5D; Supplementary Table 9). Significantly upregulated cytoskeletal proteins with over two-fold increase in GBM cells included vimentin (VIM) and IQ motif containing GTPase activating protein 1 (IQGAP1).

Subsequently, we analyzed all upregulated and exclusively found proteins in each group. The top five upregulated GOCC terms of each cell line are shown in Fig. 5E. We discovered that U87MG cells expressed more vesicular and extracellular exosome-related proteins, while more nuclear and transcription-related proteins were found in H4 cells. The heatmap compared all common cytoskeletal proteins found in H4 and U87MG cells
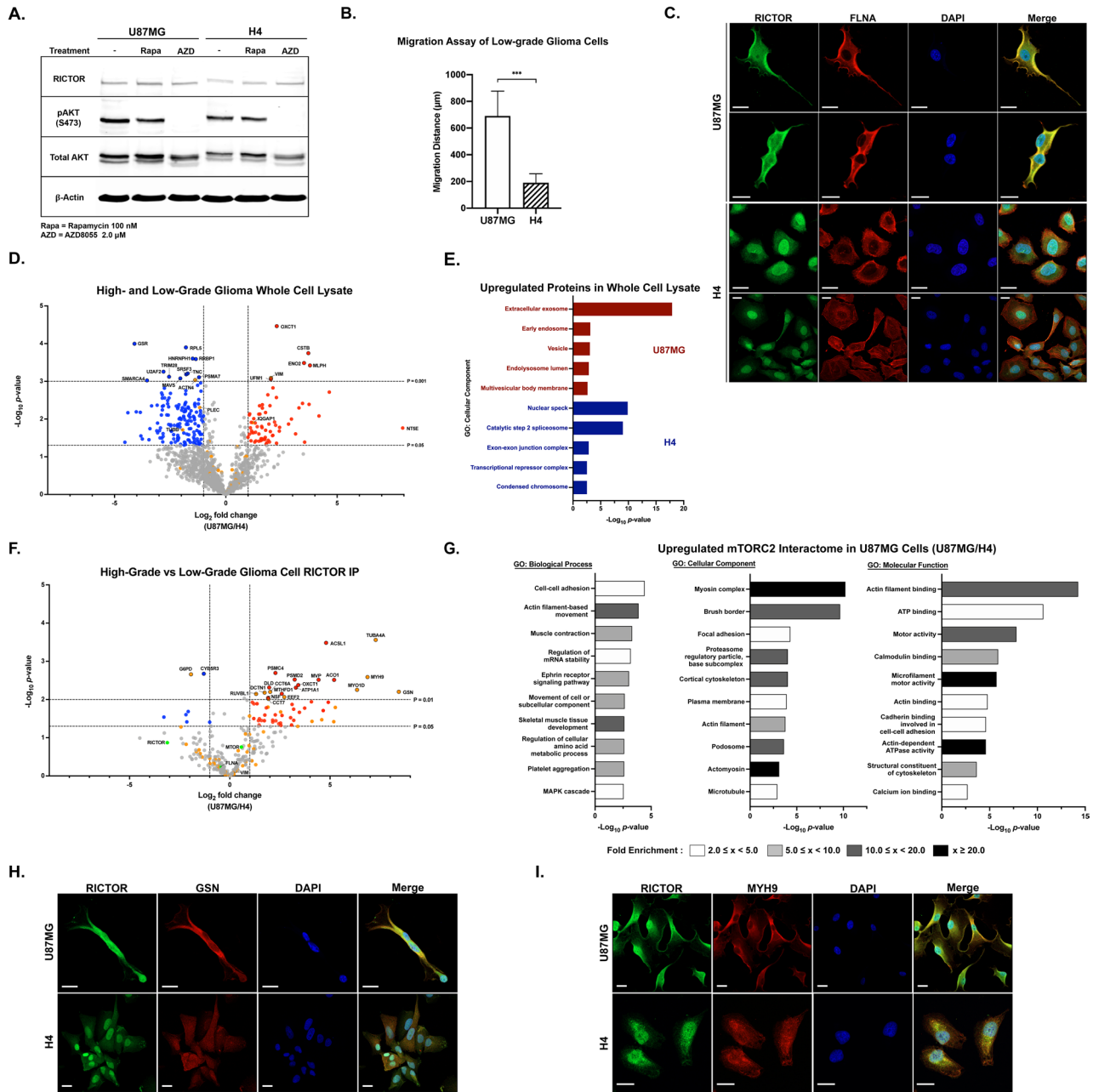
**Figure 5.** Comparative analysis of the mTORC2 interactome in high- vs. low-grade glioma cells. **(A)** Western blot of RICTOR levels and mTORC2 activities (pAKT) using U87MG and H4 cell lysates. **(B)** Comparison of migration distance between U87MG cells (experiment shown in Fig. 1F) and H4 cells under normal conditions; n = 3. All data are the mean ± SD. ***$p < 0.001$. **(C)** Immunofluorescence analysis showing different localizations of RICTOR and FLNA in U87MG and H4 cells. Scale bar = 20 μm. **(D)** Volcano plots of proteomic analysis from U87MG and H4 whole-cell lysates; n = 3 biological replicates. Proteins with $\log_2$ fold change (LFQ U87MG/H4) ≥ 1, $p < 0.05$ are highlighted in red, while proteins with $\log_2$ fold change ≤ -1, $p < 0.05$ are highlighted in blue. Proteins with $p$-values < 0.01 are shown with a black border. Statistical significance was calculated from the LFQ values of each common protein of the two conditions using an unpaired two-sided Student's t-test. All cytoskeletal proteins are shown in orange. **(E)** Gene ontology analysis showing GOCC terms of upregulated and unique proteins of the cell line comparing U87MG and H4 cells. Plots showing ten top-ranked -$\log_{10}(p$-value) GOCC terms with FDR < 0.05 of each cell line. **(F)** Volcano plots of the results of the AP-MS experiments in (J) showing changes in mTORC2-associated proteins in U87MG cells compared to H4 cells; n = 3 biological replicates. Proteins with $\log_2$ fold change (LFQ U87MG/H4) ≥ 1, $p < 0.05$ are highlighted in red, while proteins with $\log_2$ fold change ≤ -1, $p < 0.05$ are highlighted in blue. Proteins with $p$-values < 0.01 are shown with a black border. Statistical significance was calculated from the LFQ values of each common protein of the two conditions using an unpaired two-sided Student's t-test. Key mTORC2-interacting proteins are shown in green circles. All cytoskeletal proteins are shown in orange. **(G)** Gene ontology analysis of increased/presented proteins in the mTORC2 interactome of U87MG cells. Plots showing top -$\log_{10}(p$-value) GOBP, GOCC, and GOMF terms with FDR < 0.05 and the bar colors representing fold enrichment of each specific term. **(H,I)** Immunofluorescence analysis of RICTOR and GSN (M) or MYH (N) in U87MG and H4 cells. Scale bar = 20 μm.

(Supplementary Fig. 2D). The expression of most cytoskeleton-associated proteins did not show significant differences. We confirmed VIM expression by IF, and the output correlated with our proteomics data that less VIM was observed in H4 cells than in U87MG cells (Supplementary Fig. 2E). However, we speculated that the whole-cell lysate proteomic results could not specifically answer protein localization and cell migration questions. Therefore, we predicted that observing the mTORC2 interactome would provide better insights into the distinct mTORC2-mediated regulatory mechanisms of GBM cell migration.

Consequently, the mTORC2 interactomes of H4 and U87MG cells were elucidated (Supplementary Fig. 2F; Supplementary Table 10). Label-free quantification was performed among commonly found proteins, and the $\log_2$ fold changes of U87MG cells over H4 cells were demonstrated (Fig. 5F, Supplementary Table 10). We identified the proteins that explained the most remarkable differences between high- and low-grade glioma cells. We discovered that gelsolin (GSN), tubulin alpha-4A chain (TUBA4A), myosin-9 (MYH9), and unconventional myosin-Id (MYO1D) had the most considerable fold changes among all mTORC2-interacting proteins (Fig. 5F, Supplementary Fig. 2G). Interestingly, GSN, MYH9, and MYO1D had been shown in previous experiments to be highly associated with active mTORC2 in highly migratory U87MG cells and lost their interactions when cells had impaired movement.

Furthermore, we classified all upregulated and specific mTORC2 interactomes in U87MG cells compared to H4 cells. The associated GO terms consisted of various cytoskeletal structures and activities (Fig. 5G). Thus, it could be inferred that the interacting proteins more highly associated with mTORC2 in U87MG cells help promote migrational activities and potentially elevate invasiveness.

Accordingly, we investigated the relationship between GSN or MYH9 and RICTOR in both cell lines. Protein colocalization events between GSN-RICTOR and MYH9-RICTOR were observed in U87MG cells, but fewer interactions were exhibited in H4 cells. These results were similar to the AP-MS results (Fig. 5H,I).

To further prove whether GSN-RICTOR and MYH9-RICTOR interactions are associated with cell migrational control, we also determined cell migration ability in two additional cell lines, DBTRG-05MG and SW1088 representing high-grade and low-grade brain cancer cells (Supplementary Fig. 3A). The co-immunoprecipitation results showed that mTORC2 were most highly associated with GSN in U87MG followed by DBTRG-05MG which are aggressive glioblastoma cell lines. On the other hand, mTORC2 were not strongly interacting with GSN, MYH9, as well as AKT, a known mTORC2 substrate, in low-grade glioma cell lines (Supplementary Fig. 3B). Overall, the results suggested that the distinct mTORC2 interactome is one of the key factors supporting the enhanced migration characteristics of GBM cells.

### Gelsolin promotes mTORC2-mediated migration by connecting the complex to actin-binding and membrane-associated proteins to form actin-based structures.

Next, we investigated the association between mTORC2 and GSN or MYH9 in GBM cells. IF staining of RICTOR, GSN, and MYH9 in activated, starved, and AZD8055-treated U87MG cells was carried out. We found that GSN-RICTOR and MYH9-RICTOR colocalized near the plasma membrane and cytosol under mTORC2-activating conditions and rapamycin treatment. In contrast, GSN and MYH9 proteins were observed in the cytoplasm of cells while RICTOR was present in the perinuclear and nuclear regions under three mTORC2-inactivating states: serum-starved, AZD8055-treat, and treatment with an mTORC2-specific inhibitor, JR-AB2-011 (Fig. 6A, Supplementary Fig. 4A,B). We later knocked down *MAPKAP1* and observed the altered localization of RICTOR to the nucleus and cytosol (Fig. 6B). However, the localization of GSN and MYH9 did not appear as immensely altered as RICTOR but tended to be more evenly distributed throughout the cells. Our findings suggested that a functionally active mTORC2 is required for the protein–protein interactions and colocalization between RICTOR/GSN/MYH9 at the PM.

Finally, we comprehensively investigated GSN, the most dynamic protein among all conditions observed. To elucidate the consequences of the mTORC2-GSN interaction, we demonstrated the effects of *GSN* knockdown by 2'-deoxy-2'-fluoro-D-arabinonucleic acid antisense oligonucleotides (FANA ASO) against the *GSN* gene on the localization of RICTOR, together with the structures of F-actin networks. We found that without GSN, RICTOR distribution was dramatically affected, as the proteins were less associated with the PM and only present in the cytoplasm and nuclei. The maximal destructive effect on the F-actin network was determined when cells were treated with 10.0 μM GSN-FANA (Fig. 6C, Supplementary Fig. 4C). Overall, the results suggested that both the active mTORC2 complex near the plasma membrane and the availability of gelsolin in cells could collaboratively promote efficient GBM cell movement.

To characterize the effectors of the mTORC2-GSN connection, we performed a quantitative proteomic analysis of RICTOR IP samples under two conditions: (1) Control and (2) *GSN* knockdown. We aimed to observe all mTORC2-interacting proteins affected by GSN depletion to investigate how the mTORC2-GSN interaction can control GBM cell migration. The RICTOR-IP eluates of the control and *GSN*-knockdown groups contained partially different proteins (Supplementary Fig. 4D). The common proteins found in both conditions were selected, compared, and shown in the volcano plot (Fig. 6D, Supplementary Table 11).

The results showed that we successfully depleted GSN from mTORC2 pulldown by over four-fold. The knockdown slightly affected the total amount of immunoprecipitated mTORC2 and decreased various mTORC2-associated proteins, especially actin-binding proteins, but did not disrupt the critical components of mTORC2 (mTOR, RICTOR, MAPKAP1, and MLST8). In addition, interactions between mTORC2 and several significant direct interactors, such as ACTG1, FLNA, MYH9, MYO1D, TUBA4A, MAP1B, and PLEC, were not significantly decreased.

The top-ranked GO biological process terms of the diminished mTORC2-interacting proteins when *GSN* was knocked down were demonstrated (Fig. 6E, Supplementary Fig. 4E). Furthermore, we focused on the downregulated cytoskeleton-associated mTORC2 interactome and found that the interrupted processes included
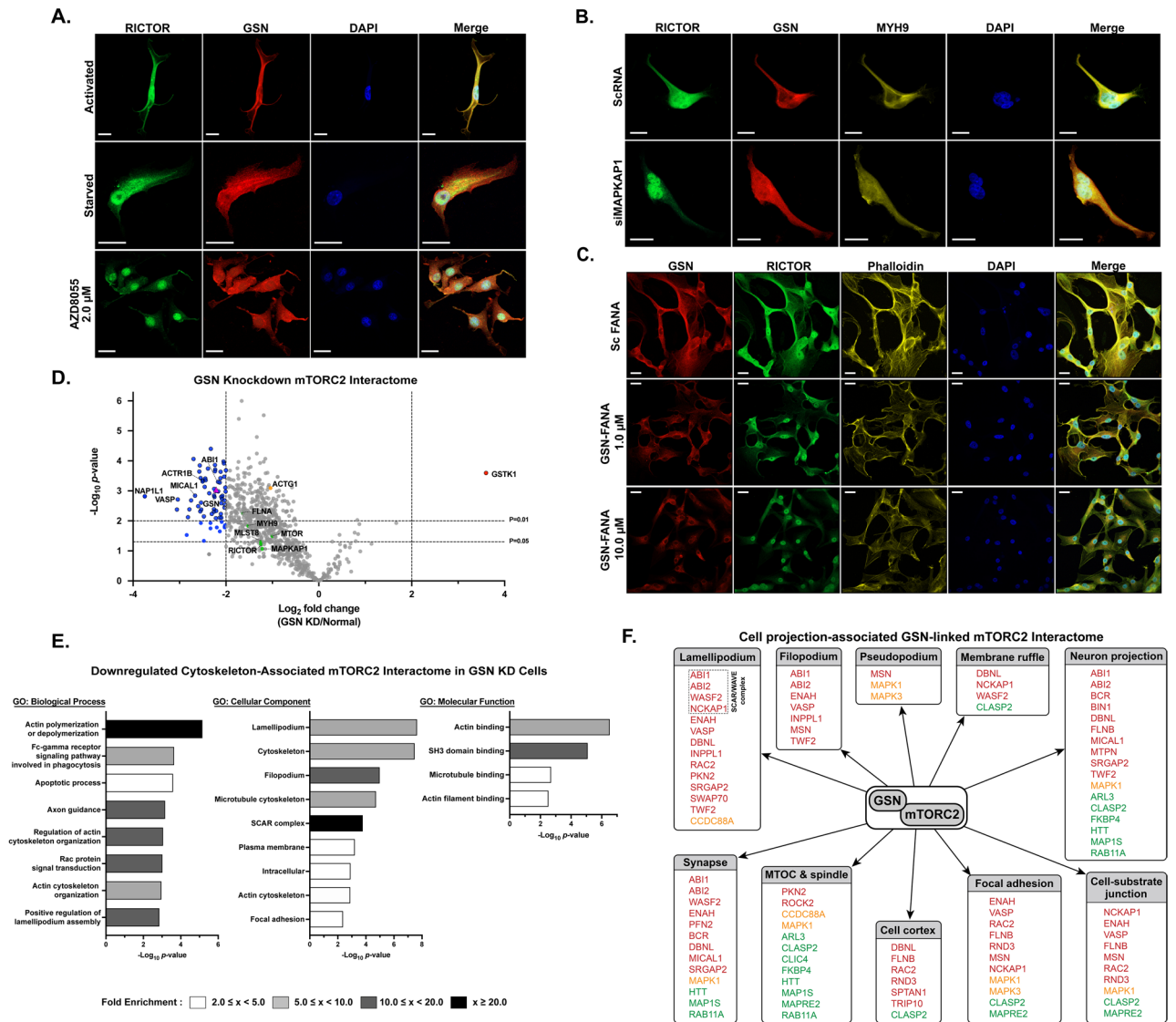
**Figure 6.** Significance of GSN in mTORC2-mediated cell migrational control. (**A**) Immunofluorescence staining of U87MG cells showing localization of RICTOR and GSN under activation, serum starvation, and inhibition conditions. Scale bar = 20 μM. (**B**) Immunofluorescence staining of U87MG cells showing colocalization of RICTOR, GSN, and MYH9 under control and *MAPKAP1* knockdown conditions. (Sc: scrambled siRNA). Scale bar = 20 μm. (**C**) Immunofluorescence staining showing localization of GSN and RICTOR and F-actin arrangement in U87MG cells after *GSN* knockdown (1.0 μM and 10.0 μM of GSN-FANA) compared to scrambled FANA control. Scale bar = 20 μm. (**D**) Volcano plot of the results of AP-MS experiments showing changes in mTORC2-interacting proteins; n = 3 biological replicates. Proteins with $\log_2$ fold change (LFQ GSN KD/normal) ≥ 2, $p < 0.05$ are highlighted in red, while proteins with $\log_2$ fold change ≤ -2, $p < 0.05$ are highlighted in blue. Proteins with $p$-values < 0.01 are shown with a black border. Statistical significance was calculated from the LFQ values of each common protein of the two conditions using an unpaired two-sided Student's t-test. Key mTORC2-interacting proteins are shown in green circles. GSN is shown in a purple triangle. (**E**) Gene ontology analysis of decreased/absent proteins in the mTORC2 interactome of the *GSN* knockdown group. Plots showing top-ranked $-\log_{10}(p\text{-value})$ GOBP, GOCC, and GOMF terms with FDR < 0.10 and the bar colors representing fold enrichment of each specific term. (**F**) Diagram showing the GSN-linked mTORC2 interactome associated with cell projection structures. (red: MF-associated proteins, green: MT-associated proteins, yellow: MF-MT-associated proteins).

multiple actin cytoskeleton-related activities. The negatively affected cellular components mainly comprised the cytoskeletal structures supporting cell protrusion. With all the information, we developed a final network showing effector proteins linked to mTORC2 through GSN or the cell projection-associated GSN-linked mTORC2 interactome. (Fig. 6F). Our findings help elucidate the PPI network between mTORC2 and specific proteins, enabling mTORC2 to regulate cytoskeletal remodeling and facilitate cell projection.

Finally, we performed RICTOR IP to immunoprecipitate mTORC2 in U87MG cells under four culturing conditions varying mTORC2 activation states: normal, serum activation, AZD8055 treatment, and JR-AB2-011

treatment. The immunoblotting results demonstrated that active mTORC2 substantially interacted with GSN and MYH9. In addition, we also demonstrated that active mTORC2 interacted more with actin-binding proteins representing important players in the actin reorganization process, including moesin (MSN), vasodilator-stimulated phosphoprotein (VASP), and cofilin (CFL) as shown in Supplementary Fig. 5A. We further confirmed that when U87MG cells lack GSN, the cell migration ability was negatively affected (Supplementary Fig. 5B). In conclusion, the oveall results supported our findings from mass spectrometry analyses.

**Major mTORC2 interactome determines complex functions in invasive brain cancer cells.** We proposed a schematic diagram of how active mTORC2 could extensively promote the superior cell migration ability of GBM cells (Fig. 7A). When activated through linkage with GSN, mTORC2 interacts with many actin-binding proteins and microtubule-associated proteins involved in forming dynamic protrusive structures, such as filopodia and lamellipodium. Conversely, inactive mTORC2 complexes interact more with intermediate filament proteins, resulting in a less motile phenotype.

We eventually compared the proteins in the mTORC2 interactome identified by every protein separation and digestion method (Supplementary Fig. 6). There were 101 proteins commonly found in all three groups, including RICTOR, mTOR, and MAPKAP1 (Supplementary Table 12). All proteins matched with the list obtained from the knockdown experiment were selected and finalized into 88 proteins directly associated with RICTOR (Fig. 7B). Apart from the core components of mTORC2, 86 other stable interacting partners of mTORC2 can be categorized into several groups responsible for essential biological processes. To summarize, the results from this study provide more insights into several other aspects of mTORC2 functions in highly invasive glioblastoma, although they mainly highlight the cell migration process. It could further initiate many more investigations on the mechanistic regulation of this multiprotein complex and lead to a better understanding of brain cancer biology.

## Discussion

Glioblastoma multiforme has been depicted as a highly invasive, aggressive, and incurable cancer[4,45,46]. This study extensively shows that mTORC2 plays a critical role in GBM migration through the direct regulation of cytoskeleton dynamics. mTORC2 inhibition by AZD8055 treatment or *RICTOR* knockdown and mTORC2 inactivation by starvation dramatically affect cell migration, actin cytoskeleton, and microtubule organization in GBM cells. Several previous studies have shown that mTORC2 inactivation or ablation could inhibit the migration of many cell types, including cancers[47–51].
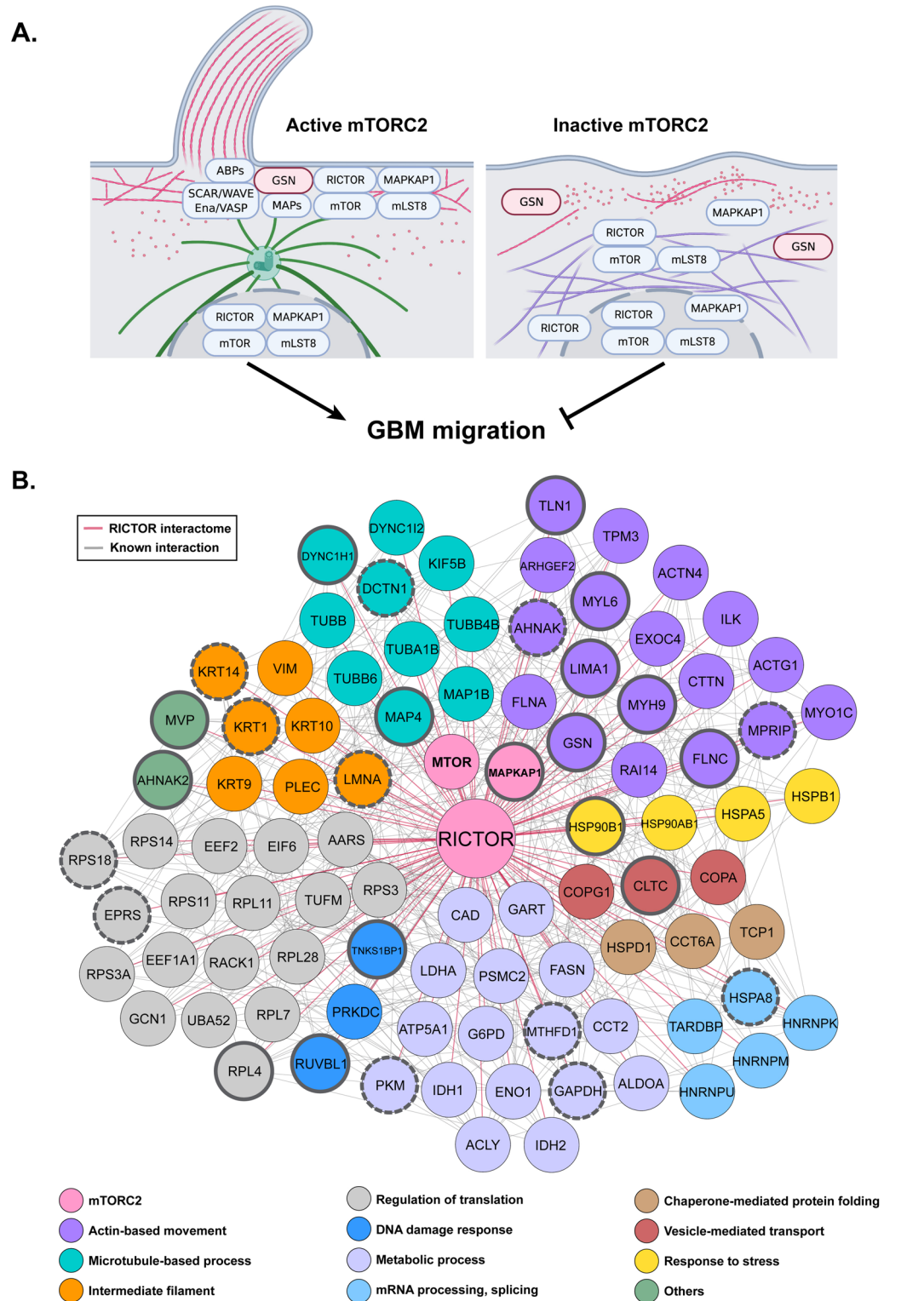
Here, we define that RICTOR localization can be used to distinguish glioma cell migrational phenotypes in an mTORC2 activity status-dependent manner. Activation of mTORC2 is critically dependent on its key components, RICTOR and MAPKAP1[42]. The binding of MAPKAP1 initiates the complex integrity of mTORC2 to the PM. Additionally, the association of the PH domain of MAPKAP1 with phosphatidylinositol 3,4,5-trisphosphate (PIP3) at the membrane has been shown to regulate mTORC2[38,52]. Ebner et al. have shown that localization of mTORC2 activity can be observed near the plasma membrane, in mitochondria, and in some endosomal vesicles[36]. Furthermore, cytoplasmic and nuclear translocation of mTORC2 components has been determined[35]. Even though nuclear or perinuclear mTORC2 function is still elusive[10,53], our results support the translocation of mTORC2 in GBM when mTORC2 is inactivated, resulting in less plasma membrane-bound and more nuclear and perinuclear mTORC2.

Since oncogenic signal transduction may differ from the canonical pathway, resulting in novel protein–protein interactions[54], we integrated quantitative proteomic analysis with modified culturing conditions to vary mTORC2 activation states. This study describes the dynamic mTORC2 interactome identified from quantitative AP-MS analyses in GBM. We demonstrate that mTORC2 activity status defines mTORC2-interacting partners, affecting glioblastoma cell migration ability.

Cytoskeletal remodeling is an essential process supporting cancer migration and invasion. Deregulated cellular architecture results in increased formation of various protrusive structures, such as lamellipodia, filopodia, and invadopodia, affecting cancer cell migration and leading to metastasis[55,56]. All types of cytoskeletons play pivotal roles in promoting this cancerous behavior[55]. Moreover, crosstalk between the actin cytoskeleton and microtubules has been highlighted in cancers[57]. Our study demonstrates that mTORC2 is one of the master regulators of GBM migration and a central complex connecting numerous cytoskeletal proteins to modulate cytoskeletal network dynamics by promoting physical interactions between significant players. To elucidate the impact of the mTORC2 interactome on the enhanced cell migrational control of highly invasive brain cancer, we differentially characterized the mTORC2 interactome in GBM compared to nonmalignant astrocytoma utilizing the AP-MS technique. mTORC2-GSN is among the most distinguishable interactions between high- and low-grade cells.

GSN is an important $Ca^{2+}$-dependent regulator of the actin cytoskeleton. It serves as an actin filament severing and capping protein and promotes actin cytoskeleton turnover[58]. GSN is one of the most abundant actin-binding proteins (ABPs). Its dysregulation has been involved in several pathological conditions in humans, including multiple types of cancers[59–64]. GSN has also been implicated as a regulator promoting cancer cell migration, invasion, and epithelial-mesenchymal transition (EMT)[60,65–69]. Investigation of GSN or gelsolin-like proteins in human gliomas has been reported in several studies as candidate biomarkers for clinical samples[32,70–73]. However, the molecular and biological functions of GSN in brain cancer have not been clearly defined.

The molecular mechanism of GSN-mediated actin polymerization and regulation of cell migration is through the binding of phosphatidylinositol 4,5-bisphosphate (PI(4,5)P2), which has gelsolin-uncapping properties leading to actin filament elongation[74,75]. GSN severing activity can also be controlled and suppressed by phosphatidylinositol 3,4,5-trisphosphate (PI(3,4,5)P3). Moreover, structural changes in mTORC2 located at the PM leading

**Figure 7.** Roles of the mTORC2 interactome in cell migrational control and others. **(A)** Diagram of the active mTORC2 function in controlling glioblastoma cell migration via RICTOR-GSN interaction by recruiting actin-binding proteins and microtubule-associated proteins to form cell protrusion structures (left). Under inactivation conditions, mTORC2 loses MAPKAP1 and interacts with intermediate filament proteins (right). (red: actin cytoskeleton, green: microtubule, purple: intermediate filaments). The graphic was created by Biorender.com. **(B)** Diagram showing the final 86 mTORC2 stable interactomes commonly identified from all methods. Proteins were categorized into groups depending on their primary functions and associated biological processes. Pink lines indicate novel interactions. Circles with bold borders represent the dynamic mTORC2 interactome upregulated (solid line) or downregulated (dashed line) in migrating glioblastoma cells.

to constitutive activation can be induced by PI(3,4,5)P3[10]. Loss of PI3Kα, the key PIP3-producing enzyme, increases gelsolin-mediated actin-severing activities[76].

Recent studies have described the involvement of phosphatidylinositol 3,4,5-trisphosphate 5-phosphatase 2 (INPPL1) in the migration and metastasis of breast cancer and glioblastoma cells. INPPL1 can dephosphorylate PIP3 and PI(4,5)P2, while its inhibition increases glioblastoma migration[77–79]. We also identified INPPL1 in the mTORC2 interactome, and its level was affected by *GSN* knockdown. Our results suggest that the mTORC2-GSN interaction might prevent or delay the catalytic activities of INPPL1. Therefore, one plausible mechanism of how mTORC2 could promote actin polymerization activity is increased PIP2 suppressing GSN-severing activity.

Similar to INPPL1, other proteins involved in phosphatidylinositol binding were found to be significantly decreased after *GSN* knockdown, such as coiled-coil domain containing 88A (CCDC88A), profilin-2 (PFN2), twinfilin-2 (TWF2), and phosphatidylinositol-5-phosphate 4-kinase type 2 alpha (PIP4K2A). Interestingly, CCDC88A (or girdin) has been determined to be a critical modulator of the PI3K-mTORC2-AKT signaling pathway that controls cell migration[80–82]. Hence, mTORC2 might be primarily involved in the regulation of phosphoinositide signaling. However, more studies are needed to clarify the mechanisms.

Actin polymerization at the PM of migrating cells promotes the formation of multiple protrusive structures[68]. We further deconvolute that GSN connects mTORC2 to many actin-binding proteins defined as signaling proteins of actin structures. Our data suggest that when the mTORC2-GSN linkage is disrupted, the most affected processes include actin polymerization/depolymerization, actin-based activities, and actin-microtubule association. The findings conclude that mTORC2 promotes cancer cell migration by inducing the formation of multiple types of actin structures through GSN connections. Both mTORC2 and GSN help promote the PM-localization process of each other. Additionally, exclusive cytoskeletal proteins in the mTORC2 interactome of U87MG cells include KIF3B, LIMA1, SVIL, FLNC, and MYO18A. Further studies are essential to clarify how interactions with these proteins lead to advanced GBM migration.

Finally, we identified 86 proteins that are stable interactors of mTORC2 in GBM cells and highlighted the significance of GSN. With GSN, mTORC2 can be constantly localized close to the plasma membrane. The complex also performs its known functions by activating PKCs and FLNA to generate highly dynamic networks. The stable mTORC2 interactome identified in our study could provide additional information regarding other biological roles of mTORC2 in brain cancer. However, the clinical relevance of the findings must also be validated in order to translate this basic knowledge into useful clinical applications in the future.

In summary, this study provides the novel fundamental idea of a specific regulatory mechanism of aggressive brain cancer cell migration through the relationship between mTORC2 and GSN. Additional players and other mechanistic regulations promoting glioblastoma migration ability await further investigation, which could be deciphered using quantitative proteomics and systems biology approaches.

## Materials and methods

### Cell lines.
U87MG and H4 cells were maintained in low glucose Dulbecco's modified Eagle's medium (DMEM) supplemented with 10% (vol/vol) fetal bovine serum (FBS) and 1% (vol/vol) Antibiotic–Antimycotic (Gibco) at 37 °C with 5% (vol/vol) $CO_2$. DBTRG-05MG cells were maintained in RPMI-1640 medium supplemented with 10% (vol/vol) fetal bovine serum (FBS) and 1% (vol/vol) Antibiotic–Antimycotic (Gibco) at 37 °C with 5% (vol/vol) $CO_2$. SW1088 cells were maintained in Leibovitz's L-15 Medium supplemented with 10% (vol/vol) fetal bovine serum (FBS) and 1% (vol/vol) Antibiotic–Antimycotic (Gibco) at 37 °C with 5% (vol/vol) $CO_2$. All four cell lines were purchased from ATCC. For activation conditions, cells were starved in serum-free media for 24 h before replacing the media with DMEM containing 10% FBS for another 24 h. The serum-starvation condition was performed by replacing the regular media with serum-free media for 24 h before the experiment.

### Drug treatment.
U87MG and H4 cells were cultured in low glucose DMEM containing 10% (vol/vol) FBS and 1% (vol/vol) Antibiotic–Antimycotic (Gibco) at 37 °C with 5% (vol/vol) $CO_2$ until they reached 80% confluency. The cultured cells were serum-starved in serum-free DMEM for 24 h before a 24-h treatment with rapamycin, AZD8055 (STEMCELL technologies), or JR-AB2-011 (MedChemExpress) in regular media. For live-cell imaging, U87MG cells in the drug-treated groups were serum-starved for 24 h before starting the experiment. Then, drug-containing and serum-supplemented DMEM was added to the cells for another 24 h during the imaging process.

### Gene knockdown experiment.
*RICTOR* knockdown experiments were performed using On-TARGET-plus Smartpool Human RICTOR siRNA or On-TARGETplus Non-targeting Control Pool (Dharmacon) and transfected into U87MG cells using Lipofectamine™ 3000 Transfection Reagent (ThermoFisher) in Opti-MEM media (Gibco). *MAPKAP1* knockdown experiments were performed using Accell Human MAPKAP1 siRNA or Accell Non-targeting Control Pool (Dharmacon). *GSN* knockdown proteomic and immunofluorescence staining experiments were performed using 2'-deoxy-2'-fluoro-D-arabinonucleic acid antisense oligonucleotides (FANA Antisense Oligos; FANA ASOs) against *GSN* or scrambled control FANA purchased from AUM BioTech. *GSN* knockdown migration assays were performed using On-TARGETplus Smartpool Human GSN siRNA or On-TARGETplus Non-targeting Control Pool (Dharmacon) and transfected into U87MG cells using Lipofectamine™ 3000 Transfection Reagent (ThermoFisher) in Opti-MEM media (Gibco).

U87MG cells were treated with each RNAi and their scramble controls for 24 or 48 h before the experiments were performed, depending on assay types. The cell lysate was collected 48 h after siRNA treatment for the following experiments, including western blotting, immunofluorescence staining, and immunoprecipitation. For wound-healing assays, U87MG cells were treated with RICTOR siRNA or GSN siRNA 48 h prior to the starting

point. For live-cell imaging, U87MG cells were transfected with RICTOR siRNA for 24 h before the start and incubated for another 24 h while performing the experiments.

**Western blotting analysis.**　U87MG and H4 cells were seeded into 6-well plates until reaching 80% confluency before the different treatments were performed. For protein extraction, cultured cells were lysed with lysis buffer containing 1% Triton X-100, 150 mM NaCl, 20 mM Tris HCl (pH 7.4), 1 mM EDTA, and EDTA-free protease inhibitor cocktail (PIC) (Roche). Cells were lysed on ice for 15 min and centrifuged at $16,000 \times g$ for 10 min. Total protein concentrations in the whole-cell lysate supernatants were determined by the Bradford protein assay (Bio-Rad). The protein extracts from various samples (25–35 µg) were equally loaded into the SDS-PAGE gel, separated by electrophoresis, and transferred to a nitrocellulose membrane (Bio-Rad). The membranes were blocked in Odyssey® Blocking Buffer (TBS) (LI-COR) for at least 1 h at room temperature or overnight at 4 °C and then probed with primary antibodies overnight at 4 °C. Membranes were washed in TBST and then incubated with IRDye® secondary antibodies (LI-COR). The membranes were scanned on the Odyssey® CLx Imaging Systems (LI-COR). The following antibodies were used: anti-phospho-S6 (S235/236), anti-S6, anti-phospho-AKT (S473), anti-AKT, anti-phospho-MAPKAP1 (T86), anti-mTOR, anti-phospho-FLNA (S2152), anti-MSN, anti-VASP, and anti-CFL (Cell Signaling Technologies), anti-FLNA (EMD Millipore), anti-RICTOR, anti-GSN, anti-MYH9, and anti-MAPKAP1 (Abcam).

**Cell proliferation assay.**　The proliferation of U87MG and H4 cells was observed using a CellTiter 96® AQ$_{ueous}$ One Solution Proliferation Assay (Promega). Cells were cultured in a 96-well plate for 72 h under activation and AZD8055 treatment conditions. The absorbance at 490 nm was measured to determine the cell viability of each well. The average intensity to the control well ratios at 24, 48, and 72 h after the drug treatment were plotted onto the graphs using GraphPad Prism.

**Immunofluorescence.**　U87MG and H4 cells ($1 \times 10^4$ cells per well) were cultured in 8-well chamber slides (Lab-Tek). Before staining, the cells were starved, activated, or treated with AZD8055 for 24 h. For the knockdown conditions, cells were incubated with siRICTOR, siMAPKAP1, FANA-GSN, and scramble controls for 48 h prior to the steps. Cells were fixed with 4% paraformaldehyde, lysed with 0.2% Triton X buffer, blocked with 1% BSA, and incubated with primary antibodies (anti-RICTOR, anti-MAPKAP1, anti-GSN, anti-β-tubulin (Abcam), anti-mTOR, anti-VIM (Cell Signaling Technologies), anti-FLNA (Millipore), Alexa Fluor 647 Anti-MYH9 (Abcam), Alexa Fluor 488-phalloidin (Invitrogen)) overnight at 4 °C. Samples were stained with secondary antibodies, including Alexa Fluor 488, Alexa Fluor 594, Alexa Fluor 647 Anti-Rabbit antibodies, and Alexa Fluor 568 Anti-mouse antibody. A Zenon Rabbit IgG labeling kit (Invitrogen) was used to directly conjugate to primary antibodies when necessary. Nuclei of cells were stained with DAPI. Slides were mounted with ProLong anti-fade mountant (Invitrogen). Cells were visualized by an LSM800 with an Airyscan confocal microscope (Zeiss).

**Live-cell imaging of the cytoskeleton.**　To visualize the actin cytoskeleton and microtubules, U87MG cells were labeled with silicon rhodamine jasplakinolide targeting actins (SiR-Actin) and silicon rhodamine docetaxel targeting microtubules (SiR-Tubulin) (Spirochrome) at 200 nM for 3 h prior to the imaging processes. Time-lapse microscopy started at hour 0 before the treatments were administered or at hour 24 of the siRNA-treated group for 16–24 h. Images of fluorescently labeled U87MG cells were taken to observe the cytoskeletal network using time-lapse mode at 15-min intervals. Differential interference contrast (DIC) images were overlaid and combined into merged pictures. All pictures were taken by an LSM 800 with an Airyscan confocal microscope (Zeiss).

**Cell migration assays.**　*Wound-healing assays.*　U87MG, DBTRG-05MG, H4, and SW1088 cells were grown in 24-well plates in a single layer until they reached over 90% confluency. Cells in all migration assay experiments were pretreated with 10 µg/mL Mitomycin C (Sigma-Aldrich) for 1 h. One scratch per well was made using a small plastic pipette tip, creating an approximately 1000 µm-wide gap. The first images of each sample were taken at hour 0. In the activation condition, U87MG cells were serum-starved for 24 h before a scratch was made, then serum-supplemented DMEM was added back at hour 0 of the assay. U87MG cells under starvation condition were maintained in serum-supplemented DMEM until the scratch was made, then serum-free DMEM was added back at hour 0 of the assay. Administration of AZD8055 (2.0 µM), rapamycin (100 nM), or JR-AB2-011 (2.0 µM) was performed after U87MG cells were serum-starved for 24 h. Serum-supplemented DMEM with each drug was added to the wells after gaps were made. For U87MG cells treated with RICTOR siRNA or GSN siRNA, the cells were preincubated with the siRNA for 48 h before the gap was made, then Opti-MEM (Gibco) was replaced with normal media. Images were acquired again after 6, 12, and 24 h.

*Live-cell imaging.*　Live-cell imaging of the cell migration assay was performed using DIC mode of an LSM800 Airyscan confocal microscope (Zeiss). Images were continuously taken from hour 0 (right after drug administration) for 14–24 h using time-lapse imaging. Cell migration tracking was performed using the TrackMate tool on the Fiji program[83]. Single-particle tracking mode was used to follow U87MG cell migration coordinately. Tracking lines were generated, and each colored line represents the migration path of a single glioblastoma cell.

The migration recovery experiment compared the 24-h starved cells and three conditions of 24-h siRICTOR treated U87MG cells. Cell migration was observed with time-lapse microscopy for 18 h. The reduced serum media containing RICTOR siRNA in the two siRICTOR-treated groups were half or entirely replaced with

regular media (low glucose DMEM with 10% FBS). Live-cell imaging was performed to investigate the recovery of migration ability of RICTOR-depleted cells after being supplemented with the serum to activate mTORC2.

**Whole-cell lysate proteomics.**　U87MG and H4 cells were cultured in 150-mm tissue culture dishes. Cells were harvested and lysed with 8 M urea, 100 mM triethylammonium bicarbonate (TEAB), 1X EDTA-free PIC (Roche), and 1X phosphatase inhibitor (Thermo Scientific™) and homogenized for 5 min. Lysates were centrifuged at 16,000 × g for 5 min at 4 °C. Protein concentrations were determined by a BCA assay (Thermo Scientific™). The protein concentration was adjusted to 10 mg/mL using lysis buffer. Proteins were reduced with 10 mM dithiothreitol for 30 min at 37 °C, subsequently alkylated in the dark with 40 mM iodoacetamide for 45 min at 25 °C, and quenched with 10 mM dithiothreitol for 15 min at 25 °C. Samples were diluted with 100 mM TEAB until they contained 0.6 M urea and digested with sequencing grade modified trypsin (Promega) using a 1:150 enzyme-to-substrate ratio at 37 °C for 16 h. The digested samples were acidified with 100% trifluoroacetic acid (TFA), with the final sample solution containing 0.5% TFA. Then, tryptic peptides were cleaned up with reversed-phase C18 solid-phase extraction (SPE) columns. The peptide concentrations were further determined by a quantitative fluorometric peptide assay (Thermo Scientific™ Pierce™). Finally, the peptides were dried using a SpeedVac (Thermo Scientific™).

**Affinity purification-mass spectrometry.**　*Immunoprecipitation of mTORC2.*　U87MG and H4 cells were cultured in 150-mm dishes under the normal, mTORC2-activating and mTORC2-inactivating conditions mentioned previously for 24 h before being harvested. Cells were collected after washing with PBS containing 1X EDTA-free PIC (Roche) and stored at − 80 °C for subsequent experiments. Endogenous proteins were studied to avoid artifact effects from cells overexpressing epitope-tagged proteins that might further ambiguously affect the PPIs and to understand all physical interactions under various culturing conditions with minimal confounding factors. To affinity purify mTORC2, we followed our original protocol with partial modifications[22]. Cells were lysed in lysis buffer (2% CHAPS, 50 mM HEPES, pH 7.4, 150 mM NaCl, 1 mM Na$_3$VO$_4$, 1X EDTA-free PIC (Roche)). The cleared supernatant after centrifugation (16,000 × g for 10 min) was mixed with anti-RICTOR antibody (Abcam) overnight at 4 °C. After that, SureBeads™ Protein A magnetic beads (Bio-Rad) were mixed with the lysate for 60 min at room temperature for affinity purification. The beads were collected and washed five times with wash buffer containing high salt (0.1% CHAPS, 50 mM HEPES pH 7.4, 300 mM NaCl, 2 mM DTT) to remove nonspecifically bound proteins. The proteins were eluted from the beads by mixing with Laemmli buffer and boiling at 95 °C for 10 min. Protein samples were separated by 8–10% SDS-PAGE. Gels were stained using Imperial Protein Stain solution (Thermo Scientific™) to visualize protein bands. Western blotting was also performed to confirm the key components of purified mTORC2.

To investigate the true mTORC2 interactome in U87MG cells, we adopted the QUICK (quantitative immunoprecipitation combined with knockdown) technique[84] and slightly modified it by performing label-free quantitative proteomic analysis instead of SILAC labeling. Experiments were performed in five replicates comparing siRICTOR-treated cells to normal U87MG cells. Co-immunoprecipitated proteins were separated by SDS-PAGE followed by in-gel digestion to identify the IP products.

*Mass spectrometry sample preparation.*　In-gel digestion.　The immunoprecipitated mTORC2 samples were fractionated by SDS-PAGE using 8% Tris–glycine gel. The gel was stained with Imperial Protein Stain solution (Thermo Scientific™). After that, the whole gel was washed with distilled water on a glass plate, and each lane was excised into eight slices for MS analysis. Each gel slice was further cut into small pieces (1 mm³) and then washed in 50% acetonitrile (ACN) in 25 mM triethylammonium bicarbonate (TEAB) buffer overnight to be fully destained and washed once again with the same buffer. All gels were dried by vacuum centrifugation. Proteins in the gel slices were reduced with 10 mM dithiothreitol (DTT) at 56 °C for 1 h, followed by alkylation with 50 mM iodoacetamide at room temperature for 45 min. Tryptic digestion in 25 mM TEAB was performed using sequencing grade trypsin (Promega) overnight at 37 °C. Peptides were eluted with 50% ACN and 1% trifluoroacetic acid (TFA), dried with a SpeedVac and stored at − 20 °C before LC–MS/MS analysis.

*GELFREE fractionation and in-solution digestion.*　The mTORC2 interactome from U87MG cells under three different conditions (starvation, activation, and inhibition) was immunoprecipitated as previously described, followed by the fractionation step using the gel-eluted liquid fraction entrapment electrophoresis (GELFREE) method[85] to ensure that all samples were equally fractionated for label-free quantitative proteomic analyses. Then, the samples were digested using the eFASP in-solution digestion protocol with trypsin[86]. For GELFREE separation, IP eluates were loaded into an 8% cartridge of the GELFREE 8100 system (Expedeon). Proteins were subsequently separated into 6 fractions. The collected samples were processed by the eFASP protocol using a 30 kDa MWCO cut-off centrifugal filter (Millipore). Laemmli buffer was exchanged into 0.2% deoxycholic acid (DCA) in 20 mM ammonium bicarbonate (ABC). Proteins were trypsin-digested on the filter after reduction and alkylation. DCA was removed by acid precipitation using TFA and three rounds of ethyl acetate extraction. Peptides were dried with vacuum centrifugation and stored at − 20 °C.

*On-bead digestion.*　To compare the mTORC2 interactome affected by gelsolin knockdown, the pulled-down proteins were digested by an on-bead digestion technique modified from previous literature[87]. We aimed to identify as many associated interacting partners as possible, including multiple layers of interactions. After the purification step, additional wash steps were performed with the beads using wash buffer I (0.05% IGEPAL CA-630, 150 mM NaCl, 50 mM Tris HCl pH 7.5, and 5% glycerol), followed by wash buffer II (150 mM NaCl, 50 mM Tris, and 5% glycerol) to remove trace amounts of detergents. During the elution step, 25 µL of elution buffer I

(2 M urea, 50 mM Tris, and 1 mM DTT, 5 ng/μL trypsin) was incubated with the beads for 30 min for partial digestion to release the mTORC2 interactome from the antibodies. Proteins were then eluted and alkylated twice with 50 μL elution buffer II (2 M urea, 50 mM Tris, and 5 mM chloroacetamide) for 30 min. Finally, the supernatants of each sample were pooled in a new tube and incubated overnight at room temperature for complete digestion. The digestion was stopped by adding 2 μL of trifluoroacetic acid (TFA). The final peptide clean-up step was performed using C18 StageTips (Empore) with Jupiter 300 (Phenomenex). Peptides were dried by SpeedVac (Thermo Scientific™) and resuspended in 0.1% formic acid for LC–MS/MS analysis.

*Mass spectrometry LC–MS/MS.*   Tryptic peptides were analyzed by a Thermo EASY-nanoLC™ 1000 System equipped with a 25-cm PepMap C18 EASY-Spray column and a Q-Exactive Plus Orbitrap mass spectrometer (Thermo Scientific™) with a flow rate of 300 nL/min over a 90-min gradient. The sample injection volume was 10 μL. Solvent A was 0.1% formic acid (FA) in water, and solvent B was 0.1% FA in acetonitrile. The gradient was ramped from 5 to 15% solvent B for 45 min, then increased from 15 to 40% within 8 min, then jumped to 95% in 2 min, and remained at 95% for 5 min. Eluted peptides from nano-LC were sprayed into the orbitrap mass spectrometer at 2.5 kV capillary voltage in the positive ion mode and 255 °C capillary temperature. MS/MS was operated at Top 10 data-dependent acquisition (DDA). For the full MS scans, 75,000 resolution, target ion at $1 \times 10^6$, and maximum IT of 120 ms were chosen. For the MS/MS mode, 12,500 resolution, $3 \times 10^4$ AGC, and 25 ms maximum IT were set. An isolation window was set to 1.2 m/z. The normalized collision energy was used at 27. The dynamic exclusion was set at 30 s with a dynamic fixed first mass.

*LC–MS/MS data processing.*   The proteome database search was performed by MaxQuant 1.6.2.1 with the Andromeda algorithm[88,89] against the human SwissProt proteome and common contaminants (http://www.thegpm.org/crap/) databases. The search allowed up to 2 missed cleavages with a mass tolerance of 10 ppm and 0.02 Da for MS1 and MS2, respectively. Carbamidomethylation (C) as a static modification and oxidation (15.994915@M), phosphorylation (79.966331@S, T, Y) and ubiquitination (114.042927@K) as variable modifications were included. The second peptide, dependent peptide, and match between runs were enabled. The match between run features was set at a 0.7 min time window and a 20 min alignment window. The false discovery rate (FDR) was controlled at 1%.

*Label-free quantitative proteomic analysis.*   Label-free quantitation (LFQ) by spectral counting was enabled without normalization in the MaxQuant 1.6.2.1 program in the experiments requiring quantitative analyses. Statistical analysis was performed by Perseus 1.6.0.2 software[90] with no imputation. All LFQ intensities involved in the bioinformatics analysis were $\log_2$-transformed. Proteins identified by site and reverse matches were removed. To quantify the relative changes of each identified protein, the spectral counting value of each condition was compared to another condition. First, we expected to identify all mTORC2-associated proteins present in normal IP samples but appeared to be over two-fold decreased or absent in the *RICTOR* knockdown IP samples of at least three out of five replicates.

To compare the mTORC2 interactome between the two cellular conditions: starvation and activation or activation and AZD8055 treatment. We also performed label-free quantitative proteomic analysis. Only proteins detected in all three repeats passed our filtering criteria for selected candidates. Proteins that were significantly increased or decreased by at least two-fold (*p*-value < 0.05) or unique (absent in two or all repeats of the compared group) under certain conditions might be correlated with specific mTORC2 functions responsible for cell migratory phenotypes.

In the proteomic analysis comparing U87MG and H4 proteins, $\log_2$ LFQ values of the candidate proteins found in three biological replicates were used to generate heatmaps using Java TreeView Cluster 3.0 with average linkage clustering. All proteins on the list acquired significant *p*-values (*p* < 0.05) when compared between the two groups. The cell lysate heatmap was generated from cytoskeletal proteins commonly found in the lysates. In addition, the IP heatmaps showed common mTORC2-associated cytoskeletal proteins identified from the immunoprecipitated samples of U87MG and H4 cells.

Finally, to identify GSN-linked mTORC2-associated proteins, we immunoprecipitated mTORC2 from GSN-knockdown cells compared to wild-type U87MG cells. In this case, we prepared AP-MS samples using the on-bead digestion method to reduce the loss of GSN-associated mTORC2-interacting proteins co-purified with RICTOR. To consider which proteins are linked to mTORC2 through GSN, we set up the filtering criteria that the amount of each candidate protein should be decreased in the GSN-knockdown condition at least relatively equal to or less than GSN itself ($\log_2$ fold change GSN KD/normal < -2) when compared to the control group. We hypothesized that these specific proteins could not physically link to mTORC2 without GSN.

**Protein–protein interaction network construction.**   *Gene ontology analysis.*   We characterized the mTORC2 interactome using DAVID Bioinformatics Resources 6.8 tools[91,92] and then annotated the mTORC2-associated gene ontologies by comparing our protein list to the glioma proteome as a background in the enrichment analysis to avoid tissue-specific enriched terms. The background list includes 6359 proteins derived from a combination of all identified proteins from every mass spectrometry experiment that we performed using glioma cell lines (U87MG and H4), including both whole-cell lysate and immunoprecipitated samples. To compare mTORC2 IP under different treatment conditions, we used the background list of 2083 proteins identified from all immunoprecipitated experiments under any treatment conditions to narrow it down to only highly significant GO terms related to the activation or inhibition of the mTORC2 pathway. Every protein in the background list must be found in at least three replicates. After performing the analysis, we reported the most significant candidate GO terms. All selected GO terms must have high confidence passing 5% or 10% FDR. The protein

network interactomes were constructed in Cytoscape v3.8.0 software[93]. The known protein–protein interactions among all candidate RICTOR interacting partners were imported using the GeneMANIA App based on protein colocalization and physical interactions. Redundant edges were removed, and novel edges were highlighted.

**Quantification and statistical analysis.** The data represented in the graphs are the mean $\pm$ SD. The number of experiments (n) shown in the figure legends refers to biological replicates or experimental replicates, depending on the appropriateness. All statistical analyses were performed using GraphPad Prism 9. The significance of all statistical analyses was considered significant when passing the 95% confidence level (* $p < 0.05$, ** $p < 0.01$, *** $p < 0.001$, **** $p < 0.0001$). The unpaired two-tailed Student's t-test was used when comparing two independent groups. Two-way ANOVA and ordinary one-way ANOVA with Tukey's multiple comparisons test were used to compare multiple groups with single or multiple parameters. For gene ontology, the false discovery rate (FDR), p-values, and fold enrichment values were calculated by DAVID Bioinformatics Resources 6.8 tools[91,92].

## Data availability
All data and materials are available in the manuscript, supplementary files, and raw data repositories or are available from the corresponding author upon reasonable request.

## Software availability
Raw and MaxQuant-processed proteomics data have been deposited to the PRIDE ProteomeXchange repository (https://www.ebi.ac.uk/pride/login), with the dataset accession number PXD035256. Raw data for western blotting analysis have been deposited into Mendeley Data and are available at https://doi.org/10.17632/4dmy59w389.1.

## References
1. Louis, D. N. *et al.* The 2016 World Health Organization classification of tumors of the central nervous system: A summary. *Acta Neuropathol.* **131**, 803–820. https://doi.org/10.1007/s00401-016-1545-1 (2016).
2. Masui, K., Mischel, P. S. & Reifenberger, G. Molecular classification of gliomas. *Handb. Clin. Neurol.* **134**, 97–120. https://doi.org/10.1016/B978-0-12-802997-8.00006-2 (2016).
3. Tykocki, T. & Eltayeb, M. Ten-year survival in glioblastoma. A systematic review. *J. Clin. Neurosci.* **54**, 7–13. https://doi.org/10.1016/j.jocn.2018.05.002 (2018).
4. DeAngelis, L. M. Brain tumors. *N. Engl. J. Med.* **344**, 114–123. https://doi.org/10.1056/NEJM200101113440207 (2001).
5. Thomanetz, V. *et al.* Ablation of the mTORC2 component rictor in brain or Purkinje cells affects size and neuron morphology. *J. Cell Biol.* **201**, 293–308. https://doi.org/10.1083/jcb.201205030 (2013).
6. Masui, K. *et al.* mTOR complex 2 controls glycolytic metabolism in glioblastoma through FoxO acetylation and upregulation of c-Myc. *Cell Metab* **18**, 726–739. https://doi.org/10.1016/j.cmet.2013.09.013 (2013).
7. Wu, S. H., Bi, J. F., Cloughesy, T., Cavenee, W. K. & Mischel, P. S. Emerging function of mTORC2 as a core regulator in glioblastoma: Metabolic reprogramming and drug resistance. *Cancer Biol. Med.* **11**, 255–263. https://doi.org/10.7497/j.issn.2095-3941.2014.04.004 (2014).
8. Laplante, M. & Sabatini, D. M. mTOR signaling in growth control and disease. *Cell* **149**, 274–293. https://doi.org/10.1016/j.cell.2012.03.017 (2012).
9. Sarbassov, D. D. *et al.* Rictor, a novel binding partner of mTOR, defines a rapamycin-insensitive and raptor-independent pathway that regulates the cytoskeleton. *Curr. Biol.* **14**, 1296–1302. https://doi.org/10.1016/j.cub.2004.06.054 (2004).
10. Fu, W. & Hall, M. N. Regulation of mTORC2 signaling. *Genes* https://doi.org/10.3390/genes11091045 (2020).
11. Oh, W. J. & Jacinto, E. mTOR complex 2 signaling and functions. *Cell Cycle* **10**, 2305–2316. https://doi.org/10.4161/cc.10.14.16586 (2011).
12. Jacinto, E. *et al.* Mammalian TOR complex 2 controls the actin cytoskeleton and is rapamycin insensitive. *Nat. Cell Biol.* **6**, 1122–1128. https://doi.org/10.1038/ncb1183 (2004).
13. Masui, K., Cavenee, W. K. & Mischel, P. S. mTORC2 in the center of cancer metabolic reprogramming. *Trends Endocrinol. Metab* **25**, 364–373. https://doi.org/10.1016/j.tem.2014.04.002 (2014).
14. Das, G., Shiras, A., Shanmuganandam, K. & Shastry, P. Rictor regulates MMP-9 activity and invasion through Raf-1-MEK-ERK signaling pathway in glioma cells. *Mol. Carcinog.* **50**, 412–423. https://doi.org/10.1002/mc.20723 (2011).
15. Masui, K., Kato, Y., Sawada, T., Mischel, P. S. & Shibata, N. Molecular and genetic determinants of glioma cell invasion. *Int. J. Mol. Sci.* https://doi.org/10.3390/ijms18122609 (2017).
16. Guertin, D. A. *et al.* mTOR complex 2 is required for the development of prostate cancer induced by Pten loss in mice. *Cancer Cell* **15**, 148–159. https://doi.org/10.1016/j.ccr.2008.12.017 (2009).
17. Tanaka, K. *et al.* Oncogenic EGFR signaling activates an mTORC2-NF-kappaB pathway that promotes chemotherapy resistance. *Cancer Discov.* **1**, 524–538. https://doi.org/10.1158/2159-8290.CD-11-0124 (2011).
18. Magee, J. A. *et al.* Temporal changes in PTEN and mTORC2 regulation of hematopoietic stem cell self-renewal and leukemia suppression. *Cell Stem Cell* **11**, 415–428. https://doi.org/10.1016/j.stem.2012.05.026 (2012).
19. Sticz, T. *et al.* mTOR activity and its prognostic significance in human colorectal carcinoma depending on C1 and C2 complex-related protein expression. *J. Clin. Pathol.* **70**, 410–416. https://doi.org/10.1136/jclinpath-2016-203913 (2017).
20. Jiang, W. *et al.* RICTOR expression in esophageal squamous cell carcinoma and its clinical significance. *Med. Oncol.* **34**, 32. https://doi.org/10.1007/s12032-017-0894-5 (2017).
21. Bian, Y. *et al.* Elevated Rictor expression is associated with tumor progression and poor prognosis in patients with gastric cancer. *Biochem. Biophys. Res. Commun.* **464**, 534–540. https://doi.org/10.1016/j.bbrc.2015.07.001 (2015).
22. Chantaravisoot, N., Wongkongkathep, P., Loo, J. A., Mischel, P. S. & Tamanoi, F. Significance of filamin A in mTORC2 function in glioblastoma. *Mol. Cancer* **14**, 127. https://doi.org/10.1186/s12943-015-0396-z (2015).
23. Mecca, C. *et al.* PP242 counteracts glioblastoma cell proliferation, migration, invasiveness and stemness properties by inhibiting mTORC2/AKT. *Front Cell Neurosci.* **12**, 99. https://doi.org/10.3389/fncel.2018.00099 (2018).
24. Gini, B. *et al.* The mTOR kinase inhibitors, CC214-1 and CC214-2, preferentially block the growth of EGFRvIII-activated glioblastomas. *Clin. Cancer Res.* **19**, 5722–5732. https://doi.org/10.1158/1078-0432.CCR-13-0527 (2013).

25. Li, Y. *et al.* Murine models of IDH-wild-type glioblastoma exhibit spatial segregation of tumor initiation and manifestation during evolution. *Nat. Commun.* **11**, 3669. https://doi.org/10.1038/s41467-020-17382-3 (2020).
26. Gu, Y. *et al.* mTORC2 regulates amino acid metabolism in cancer by phosphorylation of the cystine-glutamate antiporter xCT. *Mol. Cell* **67**, 128–138. https://doi.org/10.1016/j.molcel.2017.05.030 (2017).
27. Masui, K., Cavenee, W. K. & Mischel, P. S. mTORC2 and metabolic reprogramming in GBM: At the interface of genetics and environment. *Brain Pathol.* **25**, 755–759. https://doi.org/10.1111/bpa.12307 (2015).
28. Sato, T. *et al.* Mammalian target of rapamycin (mTOR) complex 2 regulates filamin A-dependent focal adhesion dynamics and cell migration. *Genes Cells* **21**, 579–593. https://doi.org/10.1111/gtc.12366 (2016).
29. Pirlog, R., Susman, S., Iuga, C. A. & Florian, S. I. Proteomic advances in glial tumors through mass spectrometry approaches. *Medicina* https://doi.org/10.3390/medicina55080412 (2019).
30. Silantyev, A. S. *et al.* Current and future trends on diagnosis and prognosis of glioblastoma: From molecular biology to proteomics. *Cells* https://doi.org/10.3390/cells8080863 (2019).
31. Kalpongnukul, N. *et al.* Phosphoproteomic analysis defines BABAM1 as mTORC2 downstream effector promoting DNA damage response in glioblastoma cells. *J. Proteome Res.* **21**, 2893–2904. https://doi.org/10.1021/acs.jproteome.2c00240 (2022).
32. Miyauchi, E. *et al.* Identification of blood biomarkers in glioblastoma by SWATH mass spectrometry and quantitative targeted absolute proteomics. *PLoS ONE* **13**, e0193799. https://doi.org/10.1371/journal.pone.0193799 (2018).
33. Smits, A. H. & Vermeulen, M. Characterizing protein-protein interactions using mass spectrometry: Challenges and opportunities. *Trends Biotechnol.* **34**, 825–834. https://doi.org/10.1016/j.tibtech.2016.02.014 (2016).
34. Chresta, C. M. *et al.* AZD8055 is a potent, selective, and orally bioavailable ATP-competitive mammalian target of rapamycin kinase inhibitor with in vitro and in vivo antitumor activity. *Cancer Res.* **70**, 288–298. https://doi.org/10.1158/0008-5472.CAN-09-1751 (2010).
35. Rosner, M. & Hengstschlager, M. Cytoplasmic and nuclear distribution of the protein complexes mTORC1 and mTORC2: Rapamycin triggers dephosphorylation and delocalization of the mTORC2 components rictor and sin1. *Hum. Mol. Genet.* **17**, 2934–2948. https://doi.org/10.1093/hmg/ddn192 (2008).
36. Ebner, M., Sinkovics, B., Szczygiel, M., Ribeiro, D. W. & Yudushkin, I. Localization of mTORC2 activity inside cells. *J. Cell Biol.* **216**, 343–353. https://doi.org/10.1083/jcb.201610060 (2017).
37. Gleason, C. E. *et al.* Phosphorylation at distinct subcellular locations underlies specificity in mTORC2-mediated activation of SGK1 and Akt. *J. Cell Sci.* https://doi.org/10.1242/jcs.224931 (2019).
38. Liu, P. *et al.* PtdIns(3,4,5)P3-dependent activation of the mTORC2 Kinase complex. *Cancer Discov.* **5**, 1194–1209. https://doi.org/10.1158/2159-8290.CD-15-0460 (2015).
39. Humphrey, S. J. *et al.* Dynamic adipocyte phosphoproteome reveals that Akt directly regulates mTORC2. *Cell Metab* **17**, 1009–1020. https://doi.org/10.1016/j.cmet.2013.04.010 (2013).
40. Yang, G., Murashige, D. S., Humphrey, S. J. & James, D. E. A Positive feedback loop between Akt and mTORC2 via SIN1 phosphorylation. *Cell Rep* **12**, 937–943. https://doi.org/10.1016/j.celrep.2015.07.016 (2015).
41. Fahey, M. E. *et al.* GPS-Prot: A web-based visualization platform for integrating host-pathogen interaction data. *BMC Bioinform.* **12**, 298. https://doi.org/10.1186/1471-2105-12-298 (2011).
42. Yang, Q., Inoki, K., Ikenoue, T. & Guan, K. L. Identification of Sin1 as an essential TORC2 component required for complex formation and kinase activity. *Genes Dev.* **20**, 2820–2832. https://doi.org/10.1101/gad.1461206 (2006).
43. Frias, M. A. *et al.* mSin1 is necessary for Akt/PKB phosphorylation, and its isoforms define three distinct mTORC2s. *Curr. Biol.* **16**, 1865–1870. https://doi.org/10.1016/j.cub.2006.08.001 (2006).
44. Jacinto, E. *et al.* SIN1/MIP1 maintains rictor-mTOR complex integrity and regulates Akt phosphorylation and substrate specificity. *Cell* **127**, 125–137. https://doi.org/10.1016/j.cell.2006.08.033 (2006).
45. Ohgaki, H. & Kleihues, P. Genetic pathways to primary and secondary glioblastoma. *Am. J. Pathol.* **170**, 1445–1453. https://doi.org/10.2353/ajpath.2007.070011 (2007).
46. Neftel, C. *et al.* An integrative model of cellular states, plasticity, and genetics for glioblastoma. *Cell* **178**, 835–849. https://doi.org/10.1016/j.cell.2019.06.024 (2019).
47. Dada, S., Demartines, N. & Dormond, O. mTORC2 regulates PGE2-mediated endothelial cell survival and migration. *Biochem. Biophys. Res. Commun.* **372**, 875–879. https://doi.org/10.1016/j.bbrc.2008.05.154 (2008).
48. Liu, L., Das, S., Losert, W. & Parent, C. A. mTORC2 regulates neutrophil chemotaxis in a cAMP- and RhoA-dependent fashion. *Dev. Cell* **19**, 845–857. https://doi.org/10.1016/j.devcel.2010.11.004 (2010).
49. Gulhati, P. *et al.* mTORC1 and mTORC2 regulate EMT, motility, and metastasis of colorectal cancer via RhoA and Rac1 signaling pathways. *Cancer Res.* **71**, 3246–3256. https://doi.org/10.1158/0008-5472.CAN-10-4058 (2011).
50. Lamouille, S., Connolly, E., Smyth, J. W., Akhurst, R. J. & Derynck, R. TGF-beta-induced activation of mTOR complex 2 drives epithelial-mesenchymal transition and cell invasion. *J. Cell Sci.* **125**, 1259–1273. https://doi.org/10.1242/jcs.095299 (2012).
51. Daulat, A. M. *et al.* PRICKLE1 contributes to cancer cell dissemination through its interaction with mTORC2. *Dev. Cell* **37**, 311–325. https://doi.org/10.1016/j.devcel.2016.04.011 (2016).
52. Gan, X., Wang, J., Su, B. & Wu, D. Evidence for direct activation of mTORC2 kinase activity by phosphatidylinositol 3,4,5-trisphosphate. *J. Biol. Chem.* **286**, 10998–11002. https://doi.org/10.1074/jbc.M110.195016 (2011).
53. Laribee, R. N. & Weisman, R. Nuclear functions of TOR: Impact on transcription and the epigenome. *Genes* https://doi.org/10.3390/genes11060641 (2020).
54. Kovalski, J. R. *et al.* The functional proximal proteome of oncogenic ras includes mTORC2. *Mol. Cell* **73**, 830–844. https://doi.org/10.1016/j.molcel.2018.12.001 (2019).
55. Aseervatham, J. Cytoskeletal remodeling in cancer. *Biology.* https://doi.org/10.3390/biology9110385 (2020).
56. Yilmaz, M. & Christofori, G. Mechanisms of motility in metastasizing cells. *Mol. Cancer Res.* **8**, 629–642. https://doi.org/10.1158/1541-7786.MCR-10-0139 (2010).
57. Dogterom, M. & Koenderink, G. H. Actin-microtubule crosstalk in cell biology. *Nat. Rev. Mol. Cell Biol.* **20**, 38–54. https://doi.org/10.1038/s41580-018-0067-1 (2019).
58. Nag, S., Larsson, M., Robinson, R. C. & Burtnick, L. D. Gelsolin: The tail of a molecular gymnast. *Cytoskeleton (Hoboken)* **70**, 360–384. https://doi.org/10.1002/cm.21117 (2013).
59. Chen, Z. *et al.* Lower expression of gelsolin in colon cancer and its diagnostic value in colon cancer patients. *J. Cancer* **10**, 1288–1296. https://doi.org/10.7150/jca.28529 (2019).
60. Deng, R. *et al.* Gelsolin regulates proliferation, apoptosis, migration and invasion in human oral carcinoma cells. *Oncol. Lett.* **9**, 2129–2134. https://doi.org/10.3892/ol.2015.3002 (2015).
61. Li, G. H., Arora, P. D., Chen, Y., McCulloch, C. A. & Liu, P. Multifunctional roles of gelsolin in health and diseases. *Med. Res. Rev.* **32**, 999–1025. https://doi.org/10.1002/med.20231 (2012).
62. Kankaya, D., Kiremitci, S., Tulunay, O. & Baltaci, S. Gelsolin, NF-kappaB, and p53 expression in clear cell renal cell carcinoma: Impact on outcome. *Pathol. Res. Pract.* **211**, 505–512. https://doi.org/10.1016/j.prp.2015.03.002 (2015).
63. Liao, C. J. *et al.* Overexpression of gelsolin in human cervical carcinoma and its clinicopathological significance. *Gynecol. Oncol.* **120**, 135–144. https://doi.org/10.1016/j.ygyno.2010.10.005 (2011).
64. Stock, A.-M. *et al.* Gelsolin Is associated with longer metastasis-free survival and reduced cell migration in estrogen receptor-positive breast cancer. *Anticancer Res.* **35**, 5277 (2015).

65. Baczynska, D., Bombik, I. & Malicka-Blaszkiewicz, M. Beta-catenin expression regulates cell migration of human colonic adeno-carcinoma cells through gelsolin. *Anticancer Res.* **36**, 5249–5256. https://doi.org/10.21873/anticanres.11095 (2016).
66. Chen, Z. Y., Wang, P. W., Shieh, D. B., Chiu, K. Y. & Liou, Y. M. Involvement of gelsolin in TGF-beta 1 induced epithelial to mes-enchymal transition in breast cancer cells. *J. Biomed. Sci.* **22**, 90. https://doi.org/10.1186/s12929-015-0197-0 (2015).
67. Van den Abbeele, A. *et al.* Downregulation of gelsolin family proteins counteracts cancer cell invasion in vitro. *Cancer Lett.* **255**, 57–70. https://doi.org/10.1016/j.canlet.2007.03.023 (2007).
68. Litwin, M. *et al.* Gelsolin affects the migratory ability of human colon adenocarcinoma and melanoma cells. *Life Sci.* **90**, 851–861. https://doi.org/10.1016/j.lfs.2012.03.039 (2012).
69. Radwanska, A. *et al.* Overexpression of lumican affects the migration of human colon cancer cells through up-regulation of gelsolin and filamentous actin reorganization. *Exp. Cell Res.* **318**, 2312–2323. https://doi.org/10.1016/j.yexcr.2012.07.005 (2012).
70. Gdynia, G. *et al.* Basal caspase activity promotes migration and invasiveness in glioblastoma cells. *Mol. Cancer Res.* **5**, 1232–1240. https://doi.org/10.1158/1541-7786.MCR-07-0343 (2007).
71. Yun, D. P. *et al.* Actin-capping protein CapG is associated with prognosis, proliferation and metastasis in human glioma. *Oncol. Rep.* **39**, 1011–1022. https://doi.org/10.3892/or.2018.6225 (2018).
72. Yang, Q. *et al.* Candidate Biomarkers and Molecular Mechanism Investigation for Glioblastoma Multiforme Utilizing WGCNA. *Biomed. Res. Int.* **2018**, 4246703. https://doi.org/10.1155/2018/4246703 (2018).
73. Ohnishi, M. *et al.* Proteomics of tumor-specific proteins in cerebrospinal fluid of patients with astrocytoma: Usefulness of gelsolin protein. *Pathol. Int.* **59**, 797–803. https://doi.org/10.1111/j.1440-1827.2009.02447.x (2009).
74. Janmey, P. A. & Stossel, T. P. Modulation of gelsolin function by phosphatidylinositol 4,5-bisphosphate. *Nature* **325**, 362–364. https://doi.org/10.1038/325362a0 (1987).
75. Szatmari, D. *et al.* ATP competes with PIP2 for binding to gelsolin. *PLoS ONE* **13**, e0201826. https://doi.org/10.1371/journal.pone.0201826 (2018).
76. Patel, V. B. *et al.* PI3Kalpha-regulated gelsolin activity is a critical determinant of cardiac cytoskeletal remodeling and heart disease. *Nat. Commun.* **9**, 5390. https://doi.org/10.1038/s41467-018-07812-8 (2018).
77. Ghosh, S. *et al.* Inhibition of SHIP2 activity inhibits cell migration and could prevent metastasis in breast cancer cells. *J. Cell Sci.* https://doi.org/10.1242/jcs.216408 (2018).
78. Elong Edimo, W. *et al.* SHIP2 controls plasma membrane PI(4,5)P2 thereby participating in the control of cell migration in 1321 N1 glioblastoma cells. *J. Cell Sci.* **129**, 1101–1114. https://doi.org/10.1242/jcs.179663 (2016).
79. Ramos, A. R., Elong Edimo, W. & Erneux, C. Phosphoinositide 5-phosphatase activities control cell motility in glioblastoma: Two phosphoinositides PI(4,5)P2 and PI(3,4)P2 are involved. *Adv. Biol. Regul.* **67**, 40–48. https://doi.org/10.1016/j.jbior.2017.09.001 (2018).
80. Wu, D., Yu, D., Wang, X. & Yu, B. F-actin rearrangement is regulated by mTORC2/Akt/Girdin in mouse fertilized eggs. *Cell Prolif.* **49**, 740–750. https://doi.org/10.1111/cpr.12285 (2016).
81. Wang, H. *et al.* GIV/girdin links vascular endothelial growth factor signaling to Akt survival signaling in podocytes independent of nephrin. *J. Am. Soc. Nephrol.* **26**, 314–327. https://doi.org/10.1681/ASN.2013090985 (2015).
82. Lin, C. *et al.* Tyrosine phosphorylation of the Gα-interacting protein GIV promotes activation of phosphoinositide 3-kinase during cell migration. *Sci. Signal.* **4**, ra64. https://doi.org/10.1126/scisignal.2002049 (2011).
83. Tinevez, J. Y. *et al.* TrackMate: An open and extensible platform for single-particle tracking. *Methods* **115**, 80–90. https://doi.org/10.1016/j.ymeth.2016.09.016 (2017).
84. Selbach, M. & Mann, M. Protein interaction screening by quantitative immunoprecipitation combined with knockdown (QUICK). *Nat. Methods* **3**, 981–983. https://doi.org/10.1038/nmeth972 (2006).
85. Tran, J. C. & Doucette, A. A. Gel-eluted liquid fraction entrapment electrophoresis: An electrophoretic method for broad molecular weight range proteome separation. *Anal. Chem.* **80**, 1568–1573. https://doi.org/10.1021/ac702197w (2008).
86. Erde, J., Loo, R. R. & Loo, J. A. Enhanced FASP (eFASP) to increase proteome coverage and sample recovery for quantitative proteomic experiments. *J. Proteome Res.* **13**, 1885–1895. https://doi.org/10.1021/pr4010019 (2014).
87. Keilhauer, E. C., Hein, M. Y. & Mann, M. Accurate protein complex retrieval by affinity enrichment mass spectrometry (AE-MS) rather than affinity purification mass spectrometry (AP-MS). *Mol. Cell Proteomics* **14**, 120–135. https://doi.org/10.1074/mcp.M114.041012 (2015).
88. Cox, J. & Mann, M. MaxQuant enables high peptide identification rates, individualized p.p.b.-range mass accuracies and proteome-wide protein quantification. *Nat. Biotechnol.* **26**, 1367–1372. https://doi.org/10.1038/nbt.1511 (2008).
89. Cox, J. *et al.* Andromeda: A peptide search engine integrated into the MaxQuant environment. *J. Proteome Res.* **10**, 1794–1805. https://doi.org/10.1021/pr101065j (2011).
90. Tyanova, S. *et al.* The Perseus computational platform for comprehensive analysis of (prote)omics data. *Nat. Methods* **13**, 731. https://doi.org/10.1038/nmeth.3901 (2016).
91. da Huang, W., Sherman, B. T. & Lempicki, R. A. Bioinformatics enrichment tools: Paths toward the comprehensive functional analysis of large gene lists. *Nucleic Acids Res.* **37**, 1–13. https://doi.org/10.1093/nar/gkn923 (2009).
92. da Huang, W., Sherman, B. T. & Lempicki, R. A. Systematic and integrative analysis of large gene lists using DAVID bioinformatics resources. *Nat. Protoc.* **4**, 44–57. https://doi.org/10.1038/nprot.2008.211 (2009).
93. Shannon, P. *et al.* Cytoscape: A software environment for integrated models of biomolecular interaction networks. *Genome Res.* **13**, 2498–2504. https://doi.org/10.1101/gr.1239303 (2003).

## Acknowledgements

## Author contributions

N.C., and P.W., and T.P. participated in the study design. N.C. and N.P. performed cell-based and imaging experiments. N.C., P.W., and N.K. performed the mass spectrometry experiments. N.C. and P.W. carried out the quantitative proteomic and bioinformatic analyses. N.C. and P.W. wrote the manuscript. P.K., C.A., T.P., F.T., and J.A.L. provided suggestions.

## Competing interests

The authors declare no competing interests.

## Additional information

**Correspondence** and requests for materials should be addressed to N.C. or T.P.

**Reprints and permissions information** is available at www.nature.com/reprints.

**Publisher's note** Springer Nature remains neutral with regard to jurisdictional claims in published maps and institutional affiliations.